

Research article

Isocyanate-free fabrication of sustainable polyurethane/POSS hybrid materials with tunable thermo-mechanical response

Piotr Stachak¹, Izabela Łukaszewska¹, Jan Ozimek¹, Konstantinos Nikolaou Raftopoulos¹,
Artur Bukowczan¹, Edyta Hebda¹, Carlos Bujalance Caldach^{1,2}, Krzysztof Pielichowski^{1*}

¹Department of Chemistry and Technology of Polymers, Faculty of Chemical Engineering and Technology, Cracow University of Technology, ul. Warszawska 24, 31-155 Krakow, Poland

²Departamento de Ingeniería Química y Nuclear, Universitat Politècnica de Valencia (UPV), Camí de Vera, S/n, 46022 Valencia, Spain

Received 14 July 2023; accepted in revised form 19 September 2023

Abstract. This work reports on the synthesis of non-isocyanate polyurethanes (NIPUs) obtained via the polyaddition of diamines: dimer fatty acid-derived diamine (DFA diamine) or polyether diamine (PPO diamine) with five-membered tri(cyclic carbonate) by a pre-polymerization method. The obtained NIPUs were further chemically modified by polyhedral oligomeric silsesquioxane (POSS) – glycidylisobutyl POSS (1epPOSS). The resulting reinforced composites, containing 5, 10 or 15 wt% 1epPOSS, were characterized in terms of their structure (FTIR, NMR, XRD), microstructure (SEM-EDS) and thermo-mechanical properties (DMA). FTIR confirmed the formation of polyurethanes, and NMR proved the chemical incorporation of 1epPOSS. XRD and SEM-EDS showed a uniform distribution of 1epPOSS in the matrix for low 1epPOSS concentration, with some agglomeration effects depending on the concentration of 1epPOSS. DMA indicated mechanical reinforcement of NIPUs based on DFA diamine. For NIPUs synthesized with PPO diamine, the composite with the highest 1epPOSS loading (15 wt%) exhibited superior mechanical properties in comparison to the pristine matrix, confirmed by both DMA and static stretching test.

Keywords: nanocomposites, prepolymer, polyurethane matrix, nanoparticle, dynamic mechanical analysis, non-isocyanate polyurethane

1. Introduction

Polyurethanes (PUs) are currently the fifth most widely used type of polymers with various applications. Their vast range of applications originates from a multitude of forms in which polyurethanes may be obtained (for example, foams, elastomers, fibers, coatings, adhesives, and other) and the possibility of tailoring their properties by selecting appropriate raw materials [1]. These materials are used in biomedicine, construction, automotive, electronics, and domestic appliances as thermosets and thermoplastics. Conventional polyurethanes are obtained

by reacting polyols with isocyanates [2]. However, studies have shown that isocyanates present some hazards to human health. Exposure to those substances causes respiratory system pathologies such as asthma [3], immune sensitization [4], sputum neutrophilia or eosinophilia [5], respiratory tract irritation [6], and skin disorders, mainly skin irritation and dermatitis [7, 8]. Furthermore, on an industrial scale, isocyanates are synthesized by amine phosgenation [9]. Phosgene is a highly toxic gas that – in similarity to isocyanates – causes pathological changes in the lungs and respiratory tract [10]. Thus, in recent studies,

*Corresponding author, e-mail: krzysztof.pielichowski@pk.edu.pl

© BME-PT

more and more attention is paid to finding alternative methods of nonisocyanate polyurethanes (NIPUs) synthesis that do not require the use of isocyanates or other phosgene derivatives.

Three main methods of NIPUs production may be distinguished: polycondensation, ring-opening polymerization, and step growth polyaddition [11]. Polycondensation, also known as transurethanisation, utilizes a vast range of compounds as monomers, involving ureas, carbamates, chloroformates, nitro compounds, oxidative amines or a combination of amines, halides and CO₂ [12]. However, some of the monomers used in polycondensation are obtained from phosgene as a precursor (for example, chloroformates) [13]. Moreover, polycondensation reactions require long reaction times, and the presence of a catalyst is necessary. Additionally, the purification of obtained products is necessary to eliminate by-products of low molecular weight. Conducting transurethanisation on a commercial scale is, therefore, rather limited [14].

An alternative way to obtain NIPUs is through ring-opening polymerization (ROP), using cyclic urethanes or cyclic ureas and cyclic carbonates as monomers. Cyclic urethanes bearing six or seven-membered rings are used as a substrate. Catalysts and high temperatures must be applied to achieve high yields of NIPU. However, ROP conducted with cyclic urethanes still involves phosgene; thus, this route does not eliminate toxic precursors in the production process. Obtaining cyclic urethanes as substrates for NIPUs by green chemistry methods is still under development [15]. On the other hand, copolymerization of cyclic carbonates with cyclic ureas is an environmentally friendly method for synthesizing

polyurethanes by ROP. Seven-membered cyclic ureas are reacted with six-membered cyclic carbonates to form [n,m] polyurethanes, where n and m are derived from the molar ratio of carbonate and urea, respectively. The process is carried out using organometallic catalysts, such as di-*n*-butylmagnesium (Bu₂Mg) [16].

The most promising method for NIPUs production is the polyaddition of diamines with five membered bis(cyclic carbonate)s [11] (Figure 1). In this route, the opening of cyclic carbonate ring leads to the simultaneous formation of urethane and hydroxyl groups, yielding compounds named poly(hydroxy urethanes) (PHUs) or hydroxy non-isocyanate polyurethanes (HNIPUs). Primary or secondary hydroxyl groups are formed close to urethane ones. The dependence of the formation of hydroxyl groups of a given reaction order is related to which bond is broken during the opening of the carbonate ring, as seen in (Figure 1).

Different routes may provide cyclic carbonates; among them, the method based on the addition of CO₂ to the oxirane group raises the most significant interest. Carbon dioxide is widely available, so using it in cyclic carbonate synthesis may be considered a useful method for its utilization. In this method, various compounds bearing oxirane rings bind CO₂ in the presence of a catalyst, resulting in five-membered cyclic carbonates. Properties of final NIPU materials may be tailored by choosing appropriate epoxy precursors for cyclic carbonate synthesis [17]. While petroleum-based compounds may be used, it is also possible to obtain cyclic carbonates from renewable sources, such as epoxidized vegetable oils. Another route of cyclic carbonates' synthesis involves diols

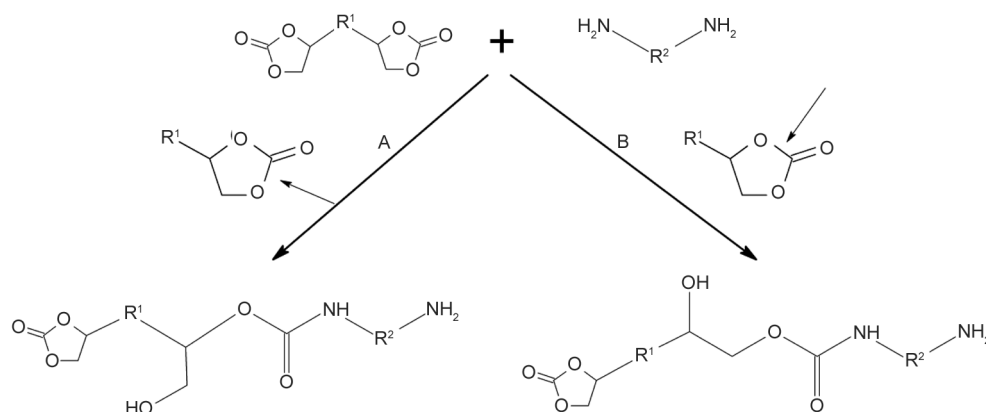


Figure 1. Possible routes of the step-growth polyaddition reaction of five-membered cyclic carbonates with amines, resulting in different order of hydroxyl groups (A: 1° OH and B: 2° OH groups). Small arrows indicate bonds that are ‘opened’ in each case.

obtained by the decomposition of biomass-derived products, such as cellulose, sorbitol, or glucose. The mentioned aspects of obtaining cyclic carbonates from epoxy compounds and CO₂ follow green chemistry postulates [18].

Non-isocyanate poly(hydroxy urethanes) often exhibit superior thermal and mechanical properties in comparison to isocyanate-derived polyurethanes, *e.g.* HNIPU foams showed better thermal insulation properties and higher tensile strength than conventional PU foams [19]. The higher thermal stability of poly(hydroxy urethanes) originates from the insusceptibility of polyaddition reaction to water. During the synthesis of conventional PUs, the presence of water leads to the formation of allophanate and biuret groups/moieties that are thermally labile and prone to hydrolytic degradation, however, no such side reactions occur in the synthesis of HNIPUs [20]. Furthermore, due to intramolecular hydrogen bonds formed by hydroxyl groups with urethane groups, poly(hydroxy)urethanes exhibit improved hydrolytic stability and improved chemical resistance [21]. It has been shown that materials with intramolecular hydrogen bonds display 1.5–2 times greater chemical resistance than those without such bonds [19]. Incorporating additives into a polymer matrix often leads to new or improved properties of nano- and micro-structured organic/inorganic hybrid materials [22]. The advantages of organic and inorganic compounds may be combined using silica-based compounds. Among various additives, polyhedral oligomeric silsesquioxanes (POSS) have attracted considerable attention [23]. Significant improvements have been observed in various properties of composites, such as better mechanical properties (enhancements in the modulus and melt strengths), higher thermal stability, higher glass transition temperature, better flame and heat resistance, improved water tolerance and dielectric properties [24]. Polymer/POSS composites have found applications in a wide variety of fields, such as coatings, surface modifiers, membrane materials or catalysts [25]. Additionally, POSS biocompatibility, non-toxicity and phase separation ability that modifies the material porosity are fundamental properties required in modern biomedical applications. Enhanced biocompatibility of POSS nanocomposite copolymers has resulted in the development of a wide range of biomedical applications, such as the development of biomedical devices, tissue

engineering scaffolds, drug delivery systems, dental applications, and biological sensors [26, 27].

Herein, we present an environmentally-friendly production path of non-isocyanate polyurethane materials via a two step process. First, tri-functional cyclic carbonate and diamines, dimer fatty acid-derived diamine or polyether diamine, were used to obtain NIPU prepolymers, which then underwent further reactions of chain extension and modification by epoxy-POSS particles to produce NIPU-glycidylisobutyl POSS (1epPOSS) nanocomposites with variable silsesquioxane content. A two-step synthesis method (prepolymerization and chain extension) was chosen to confirm the possibility of applying it in a similar manner as two-step method commonly utilized to obtain conventional polyurethane materials. Two different types of diamines were used to study the influence of their backbone chain composition on the overall properties of obtained NIPU materials, as well as their influence and interactions with 1epPOSS particles. Glycidylisobutyl POSS was chosen to be used in this work as a reactive nanofiller. Thanks to the presence of oxirane rings in its structure, it was possible to incorporate 1epPOSS into the NIPU matrices chemically. The incorporation of monofunctional 1epPOSS results in changes of the NIPU matrices by loosening the polymer network as the number of network nodes is reduced. As mentioned before, the usage of POSS particles often leads to the improvement of various chemical and physical properties of composite materials. In the case of the presented study, 1epPOSS particles were used in the NIPU-1epPOSS composite materials in order to achieve improvement in their mechanical properties. The process of 1epPOSS particle distribution in polymer matrices was studied. Fourier transform infrared spectroscopy (FTIR) was used to confirm the occurrence of the reaction between cyclic carbonate and diamines as well as chemical modification of obtained NIPU matrices with 1epPOSS particles. Importantly, a detailed nuclear magnetic resonance (¹H NMR and ¹³C NMR) investigation of NIPU matrices and NIPU-1epPOSS composite materials was conducted. X-ray diffraction (XRD) and scanning electron microscopy (SEM) techniques were used to assess amorphous or crystalline structures of obtained materials. Dynamic mechanical analysis (DMA) was used to investigate 1epPOSS influence on thermo-mechanical properties of NIPU

matrices and NIPU-1epPOSS composites. Static stretching test was also conducted to confirm mechanical reinforcement.

The combination of an environmentally-friendly method of synthesis of polyurethanes with the usage of POSS nanoparticles as reactive fillers, improving mechanical properties of NIPU matrices, stands as an important advantage in terms of the novelty and scientific significance of this work. Additionally, we hope that the detailed FTIR and NMR study presented in this paper will contribute to the better understanding of structural features of NIPU composites and hybrid materials.

2. Experimental

2.1. Materials

Cyclic five-membered trimethylpropanol tricyclocarbonate SP-3-00-003 (TMP Tricarbonate, C) was supplied by Specific Polymers (Castries, France). Diamine 1074 (dimer fatty-acid diamine, DFA diamine, P), a derivative of a dimer fatty acid (Figure 2) [28], was supplied by Croda (East Yorkshire, United Kingdom). Jeffamine D-400 (PPO diamine, J), a poly(propylene oxide) based diamine [29], was supplied by Huntsman (The Woodlands, Texas, USA). Glycidylisobutyl POSS EP041 (1epPOSS, G) was supplied by Hybrid Plastics (Hattiesburg, Mississippi, USA). 1epPOSS particles bear one reactive vertex group (epoxy), attached to POSS cage by a spacer, and seven remaining vertex groups are isobutyl. 1,4-diaminebutane D13208 (DAB, D), 1,5,7-triazabicyclo[4.4.0]dec-5-ene 345571 (TBD), *N,N'*-dimethylacetamide 8.03235 (DMAc), tetrahydrofuran 178810 (THF), tetrabutylammonium bromide 8.18839 (TBAB), tetrabutylammonium iodide 140775 (TBAI) were supplied by Sigma Aldrich (Darmstadt, Germany). Dimethylsulfoxide-*d*₆ 00905 (DMSO-*d*₆) and pyridine-*d*₅ 03403 were supplied by Deutero (Kastellaun, Germany). Hydrochloric acid was supplied by ChemPur (Piekary Śląskie, Poland), and sodium hydroxide was supplied by POCH Avantor Performance Materials Poland S.A. (Gliwice, Poland).

2.2. Synthesis

NIPU matrices were fabricated in a two-step procedure – Figure 2. In the first step, a hydroxy urethane prepolymer was synthesized with TMP Tricarbonate (C) and either DFA diamine (P) or PPO diamine (J)

which were placed into a three-necked flask that was equipped with argon inlet and outlet, thermometer, condenser, and a sampling system. The molar ratio of carbonate groups to amine groups was 2:1, and the mass of substrates was calculated so that the total mass of cyclic carbonate and long-chained amine would equal 5 g. TBD was used as a catalyst in the amount of 5 mol% (with respect to the total amount of TMP Tricarbonate, long-chained amine and 1ep-POSS if applicable). 15 ml of DMAc was used as a solvent. The reaction mixture was stirred in the temperature range between 71–77 °C. The first step of the synthesis was carried out until FTIR spectra confirmed the state of the maximum possible conversion of carbonate groups. It was indicated by two consecutive FTIR measurements having the same intensity in the carbonyl region at 1800 cm⁻¹, characteristic for the carbonyl group in the cyclic carbonate rings, in 1 h interval. In the second step, 1,4-diaminobutane (DAB, D) was added to the reaction mixture. DAB was added in such an amount so the molar ratio of carbonate groups to the sum of amine groups was 1:1. The amount of DAB was calculated by performing back titration with a pH-meter. Around 1 g of reaction mixture and a set excess of 5 ml of 0.5 M standard hydrochloric acid were added into a beaker, diluted with 10 ml of THF, sealed with parafilm and mixed for 10 min. Afterwards, the titration was performed using a 0.5 M standard solution of sodium hydroxide as a titrant. Reference titration, without adding the sample, was performed in the same manner.

The conversion rate for prepolymerization step was calculated on the basis of the titration, taking into account the initial number of moles of amine groups and the amount of amine groups after prepolymerization (Equation (1)):

$$CR = \frac{n_{\text{NH}_2}^0 - n_{\text{NH}_2}^p}{n_{\text{NH}_2}^0} \cdot 100\% \quad (1)$$

where $n_{\text{NH}_2}^0$ is the initial number of moles of amine groups, $n_{\text{NH}_2}^p$ the number of moles of amine groups after prepolymerization.

After the addition of DAB into the reaction mixture, the system was stirred for about 1.5 h, constantly being monitored by FTIR measurements. It was stopped when two consecutive FTIR measurements showed the same intensity in the carbonyl region at 1800 cm⁻¹, characteristic for carbonyl group in the cyclic carbonate rings, in 10 min interval. Then, the

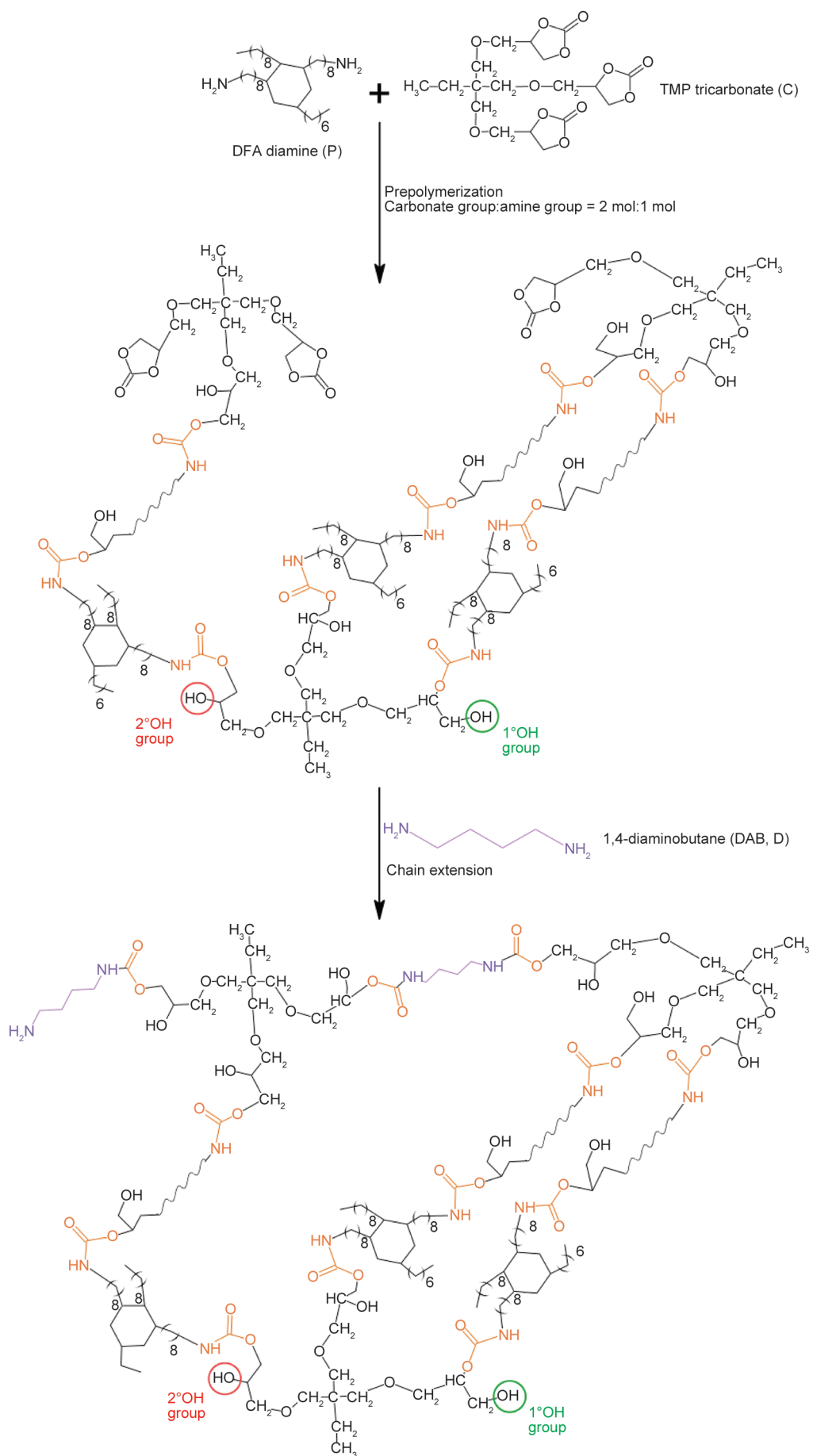


Figure 2. Two-step synthesis of NIPU based on TMP tricarcarbonate (C) and DFA diamine (P).

flask's content was transferred to a polypropylene mold and conditioned in the furnace at 110 °C for 2–4 weeks.

In the synthesis of NIPU-1epPOSS composites, 1epPOSS was introduced together with all other reagents at the beginning of the reaction, alongside with 5 mol% with respect to 1epPOSS of TBAB and TBAI mixture (1:1 mass ratio) as a catalyst promoting oxirane ring opening. 1epPOSS was added in quantities of 5, 10, or 15 wt% with respect to prepolymer mass. For the NIPU-1epPOSS materials, the molar ratio of carbonate and epoxy groups to amine groups was 2:1, and the mass of substrates was calculated so that the total mass of cyclic carbonate and long-chained amine would equal 5 g. During the chain extension step of synthesis of NIPU-1epPOSS composites, the amount of DAB was calculated in a way so that the molar ratio of the sum of carbonate and epoxy groups to the sum of amine groups was 1:1. Conversion rate for prepolymerization step for composite materials was calculated in the same manner as for NIPU matrices.

The obtained materials are listed in Table 1. Letter P in the sample code indicates that it is based on DFA diamine, and letter J that it is based on PPO diamine. The number indicates the mass fraction of 1epPOSS with respect to prepolymer mass.

2.3. Characterization techniques

Fourier-transform infrared spectroscopy (FTIR) was applied to track the reaction progress and to analyze the chemical structure of NIPU materials. The analysis was carried out using a Nicolet iS5 FTIR spectrometer equipped with the iD7 ATR Accessory, Thermo Fisher Scientific (Waltham, Massachusetts, USA). FTIR analysis was conducted in the wavenumber

range 4000–400 cm^{-1} , with a scanning resolution of 4 cm^{-1} and a data gap of 0.482 cm^{-1} .

NMR spectra were recorded with an FT-NMR 500 MHz spectrometer JNM-ECZR500 RS1 (ECZR version), JEOL Ltd. (Akishima, Tokyo, Japan). The measurement temperature was 21 °C with a pulse width of 3,6 μs , relaxation time of 4 s, and acquisition time of 3.5 s of 8 scans for ^1H proton, and 3.4 μs of pulse width, 2 s of relaxation, and 1.6 s of acquisition of 3072 scans for carbon ^{13}C resonance. DMSO- d_6 and pyridine- d_5 were used as solvents, and the spectra shift was referenced on their characteristic shift.

Wide angle X-ray diffraction (XRD) was conducted with a D2 PHASER X-ray diffractometer, Bruker (Billerica, Massachusetts, USA) equipped with the LYNXEYE XE-T detector. 2θ range was 6° to 40°, at an interval of 0.1° and acquisition time of 3 s, slit of 1 mm and shutter of 1 mm.

Scanning electron microscopy images of the obtained matrices and composite materials were recorded using a JSM-6010LA scanning electron microscope with Energy dispersive X-ray spectroscopy (EDS) function, JEOL Ltd. (Akishima, Tokyo, Japan). Images were taken of samples fractured after submersion in liquid nitrogen on the surface produced by the fracture and on the outer surfaces of the samples after removing them from the molds. The samples were coated with a layer of gold with a nominal thickness of 4 nm. The applied voltage was 10 kV and the working distance was 9 mm.

Dynamic Mechanical Analysis (DMA) was conducted with a Netzsch 242C dynamic mechanical analyzer in tension mode, NETZSCH GmbH (Selb, Germany). Measurements run in the temperature range –60 to 80 °C, at a heating rate of 2 K/min in argon atmosphere, and at a frequency of 1 Hz with an amplitude of 50 μm , up to a maximum dynamic force $F_{d, \max} = 4 \text{ N}$ and static force $F_s = 1.1 F_d$. Some samples failed earlier, in which case the measurement was stopped. The samples were rectangular pieces cut out from the solvent-cast film with an approximate thickness of 0.5 mm, width of 5 mm, and stretchable length of 7 mm. Prior to measurement, samples were dried over P_2O_5 at room temperature until equilibration of their mass.

A static stretching test was carried out using a Brookfield CT3 texture analyzer, AMETEK Brookfield (Middleborough, Massachusetts, USA), controlled

Table 1. Description of obtained NIPU-1epPOSS hybrid materials.

Sample name	Long-chained amine	Content of 1epPOSS [wt%]	Conversion of prepolymer [%]
CP0G	DFA diamine – P (Priamine 1074)	0	100
CP5G		5	100
CP10G		10	100
CP15G		15	100
CJ0G	PPO diamine – J (Jeffamine D 400)	0	99
CJ5G		5	100
CJ10G		10	98
CJ15G		15	98

by the TexturePro CT V1.8 Build 31 software from Brookfield Engineering Labs. Inc. Samples in the form of paddles, with a testing section measuring approximately 15 mm in length, 6 mm in width and 0.7 mm in thickness, were used. A tensile speed of 1 mm/s and a trigger load of 0.098 N were used. The test was conducted at room temperature ($\sim 25^\circ\text{C}$).

3. Results and discussion

3.1. Fourier transform infrared spectroscopy (FTIR) analysis

Figure 3 shows the FTIR spectra of the reference NIPUs at various stages of the synthesis. The strong band at 1800 cm^{-1} corresponds to the stretching vibrations of the carbonyl group in the cyclic carbonate rings [19]. The one at 1720 cm^{-1} is correlated to the stretching of carbonyl moieties in urethane groups [19]. The intensity of the band related to carbonate

rings decreases with the progress of the reaction (Figure 3a). At the same time, the intensities of bands corresponding to the carbonyl group in urethane linkages increase. Both of these absorption bands indicate the formation of urethane groups during the synthesis at the expense of carbonate groups. Further decrease in intensity of the band correlated to vibrations in carbonate groups is observed after adding DAB to the system. In the final product (Figure 5a), the band is almost non-existent, which indicates that nearly all carbonate groups were involved in urethane formation [16]. After chain extension, bands associated with unreacted carbonates are more pronounced in the DFA diamine-based NIPU. It may indicate that it is less reactive towards TMP Tricarbonate in comparison to PPO diamine. DFA diamine exhibits branched side chains in its structure. Although inert, long hydrocarbon side chains may

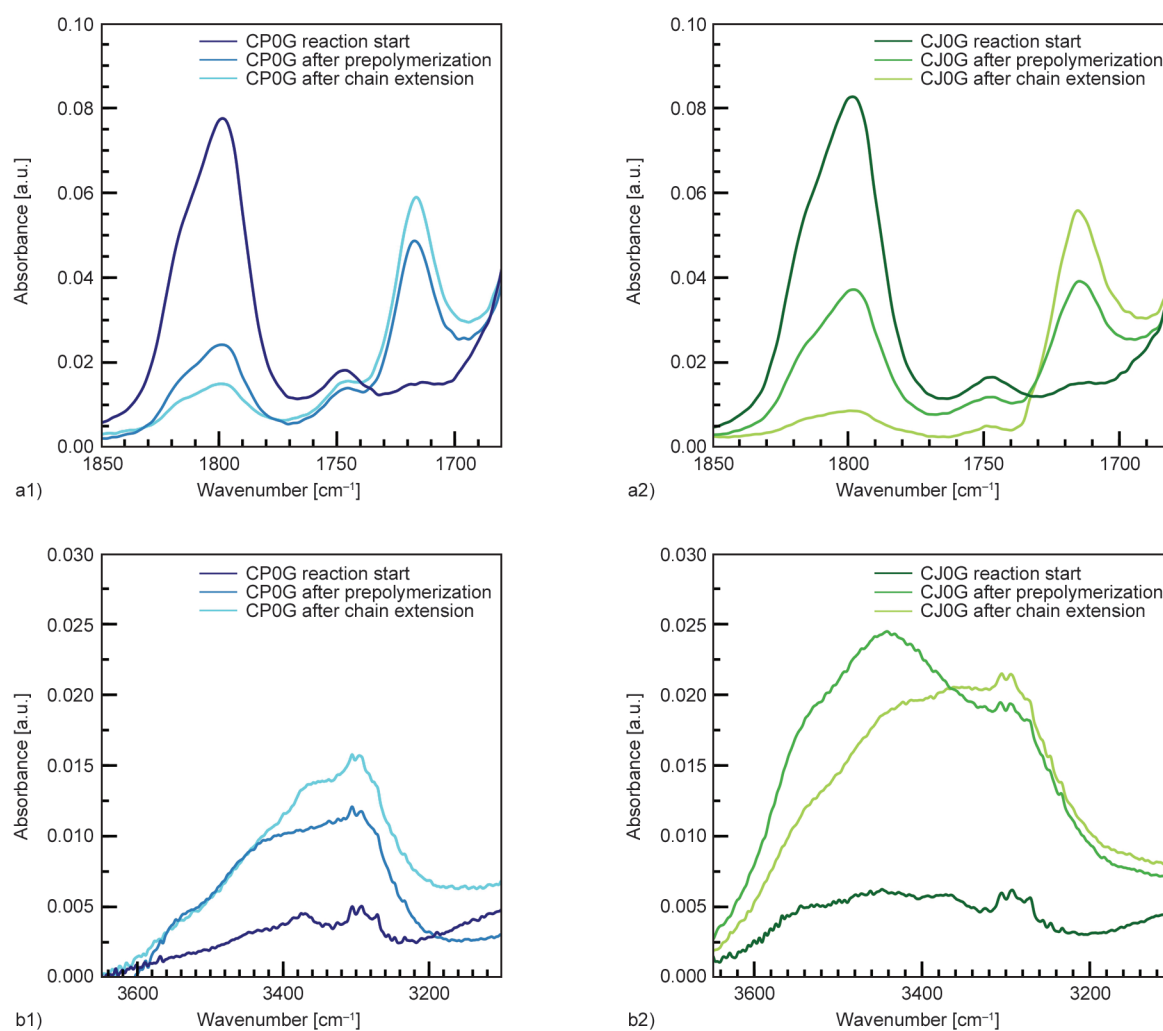


Figure 3. FTIR spectra at various stages of the synthesis of the matrices based on: a1) DFA diamine in the carbonyl region, a2) PPO diamine in the carbonyl region, b1) DFA diamine in the amine/hydroxyl region, b2) PPO diamine in the amine/hydroxyl region.

cause significant steric hindrance for carbonate rings when approaching amine-terminated chains of DFA diamine and thus contribute to its lower reactivity towards TMP Tricarbonate [30]. The broad band at 3250–3500 cm^{-1} (Figures 3b, 4b, 5b) is associated with stretching vibrations of –NH (present in urethanes) and –OH groups (formed alongside urethanes during carbonate ring opening) [15].

Figure 4 shows various stages of NIPU-1epPOSS composites synthesis for materials with 15 wt% 1epPOSS. Hydroxyurethane formation progresses in

visible in a fashion similar to the matrices (Figure 4a). Bands of stretching vibrations in the oxirane rings are observed around 840 cm^{-1} (Figure 4c). Changes in their intensity are visible only faintly during the reaction. This may support the conclusion that used 1epPOSS, bearing epoxy groups theoretically capable of reacting with the amines used in the process, is not able to react to a full extent in the carbonate-amine-1epPOSS system. Thus, it was decided to thoroughly study the changes in the bands corresponding to stretching vibrations in the oxirane ring.

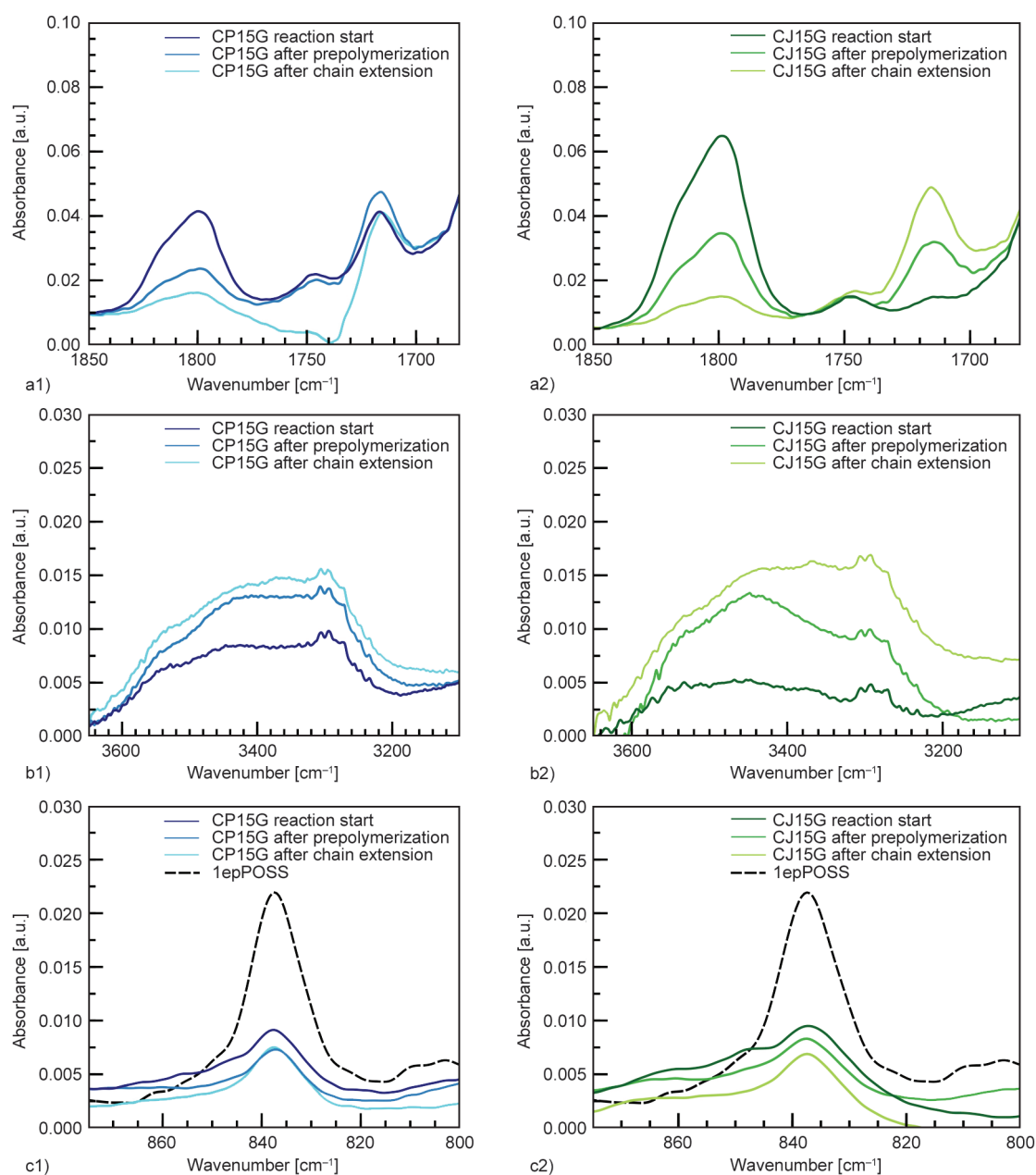


Figure 4. FTIR spectra at various stages of the synthesis of the NIPU composites with 15 wt% 1epPOSS based on: a1) DFA diamine in the carbonyl region, a2) PPO diamine in the carbonyl region, b1) DFA diamine in the amine/hydroxyl region, b2) PPO diamine in the amine/hydroxyl region, and c1) DFA diamine in the epoxy region along with spectra of pure 1epPOSS, c2) PPO diamine in the epoxy region along with spectra of pure 1epPOSS.

To do so, we carried out reactions between amines and 1epPOSS.

The spectra of NIPU matrices and NIPU-1epPOSS composites after the curing process are presented in Figure 5. Interestingly, in the cured materials, the band corresponding to carbonyls in urethane groups is observed at around 1700 cm^{-1} (Figure 5a). It is widely

reported that IR absorbance of hydrogen-bonded urethane carbonyl is observed at lower wavenumbers in comparison to carbonyl moieties, which do not form such bonds [31]. Thus, bands at 1700 cm^{-1} (Figure 5a) correspond to those C=O which are hydrogen-bonded. The hydrogen bonding may occur between urethane-derived carbonyls and secondary amine groups

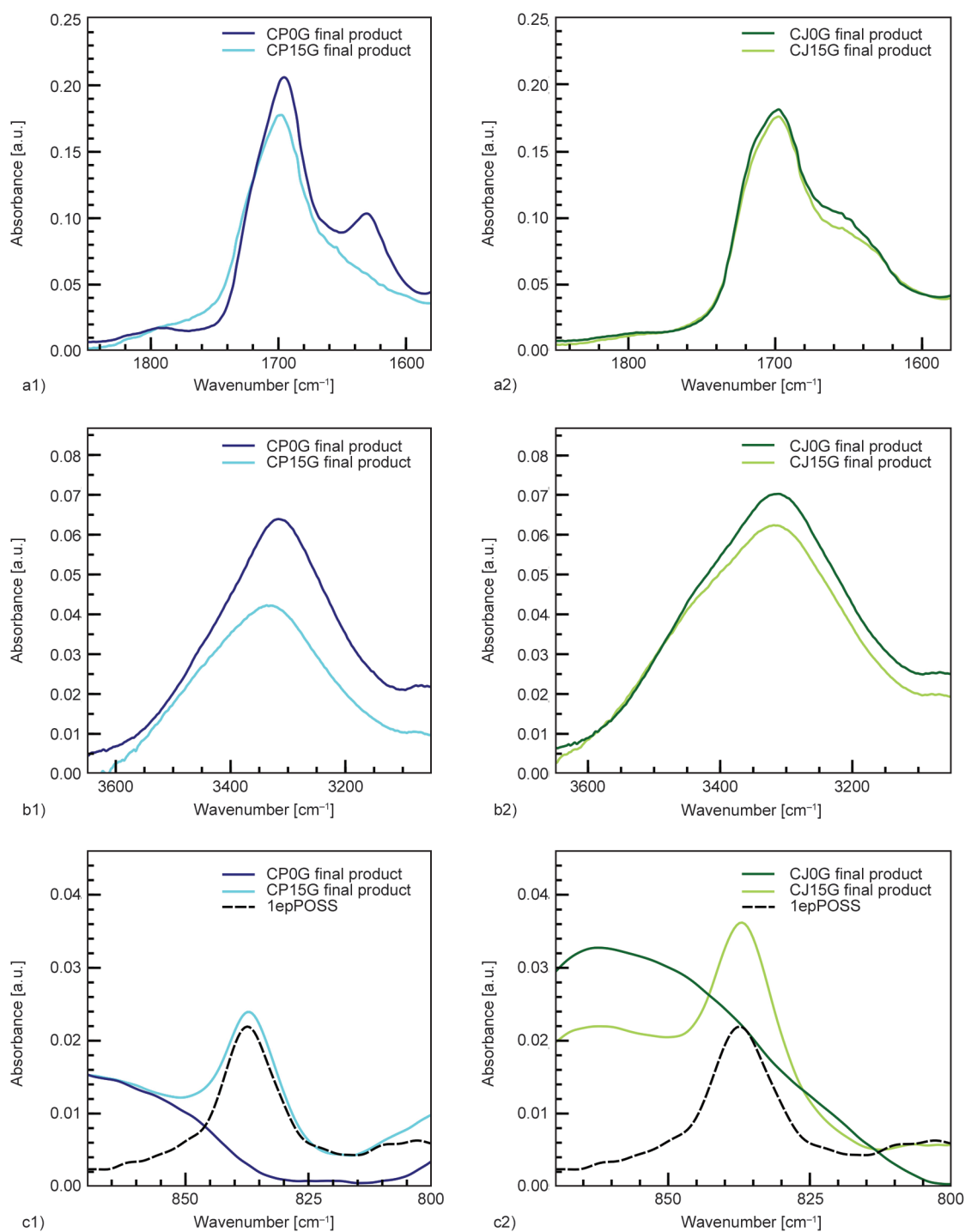


Figure 5. FTIR spectra of final products for matrices and composites with 15 wt% 1epPOSS based on: a1) DFA diamine in the carbonyl region, a2) PPO diamine in the carbonyl region, b1) DFA diamine in the amine/hydroxyl region, b2) PPO diamine in the amine/hydroxyl region, and c1) DFA diamine in the epoxy region along with spectra of pure 1epPOSS, c2) PPO diamine in the epoxy region along with spectra of pure 1epPOSS.

formed during the aminolysis of epoxy groups present in 1epPOSS. Thus, bands of hydrogen-bonded carbonyls in urethanes tend to shift towards lower wavenumbers. The formation of secondary amines may further be indicated by broadening of the region at 3250–3500 cm^{-1} (Figure 5b).

The shoulder emerging in all obtained composites' spectra at 3450 cm^{-1} is characteristic of N–H stretching vibrations in secondary amines [15]. It is more pronounced in DFA diamine-based composites in comparison to PPO diamine-based composites. Yet, it is only visible in the spectra of cured composites (Figure 5b). It may indicate the different nature of the reaction between 1epPOSS and either DFA diamine-based materials or PPO diamine-based materials.

As mentioned before, the difficulty for 1epPOSS to react with amines may be caused by steric hindrances related to the size of the silicon-oxygen cage in the silsesquioxane particles. Such geometric obstacles may prevent the effective approach of 1epPOSS molecules to the amine or urethane groups of the prepolymer. In turn, it should be possible for 1epPOSS molecules to react with DAB during the chain-extension step. Due to overlapping bands in the 3250–3500 cm^{-1} region, the formation of secondary amines is not clear enough to confirm the reaction of oxirane ring opening. Therefore, it is assumed that the lack of clear reaction signs may result from a stronger affinity of cyclic carbonate groups to amine groups

as compared to epoxy groups. The affinity of amine groups to cyclic carbonate groups over epoxy groups may promote the reaction of prepolymer chain growth in the first place, and only after the reaction is completed is it then possible for the reaction of epoxy groups with amines. In this case, the lack of visible progress of 1epPOSS epoxy groups' conversion may result from steric effects. Observable differences in reactivity towards TMP Tricarbonate between DFA diamine and PPO diamine are also noticed in the presence of 1epPOSS in the reaction system. Nevertheless, further experiments were conducted to minimize probable obstacles for the abovementioned reaction to occur.

To study the reaction between epoxy groups in 1epPOSS and the amines, reactions between those reactants were conducted with equal amounts of amine and epoxy groups without TMP Tricarbonate. Figure 6 shows an example of the reaction between DFA diamine (P) and 1epPOSS (G). The synthesis with PPO diamine (J) and DAB (D) was conducted analogously. As a result, 'building block' materials of PG 1:1, JG 1:1 and DG 1:1 were obtained. The conditions of the synthesis were similar to those of the synthesis of matrices and composites. The resulting spectra are shown in Figure 7.

A decrease in the intensity of absorption bands corresponding to stretching vibrations in the oxirane ring observed at the wavenumber 840 cm^{-1} , is evident for

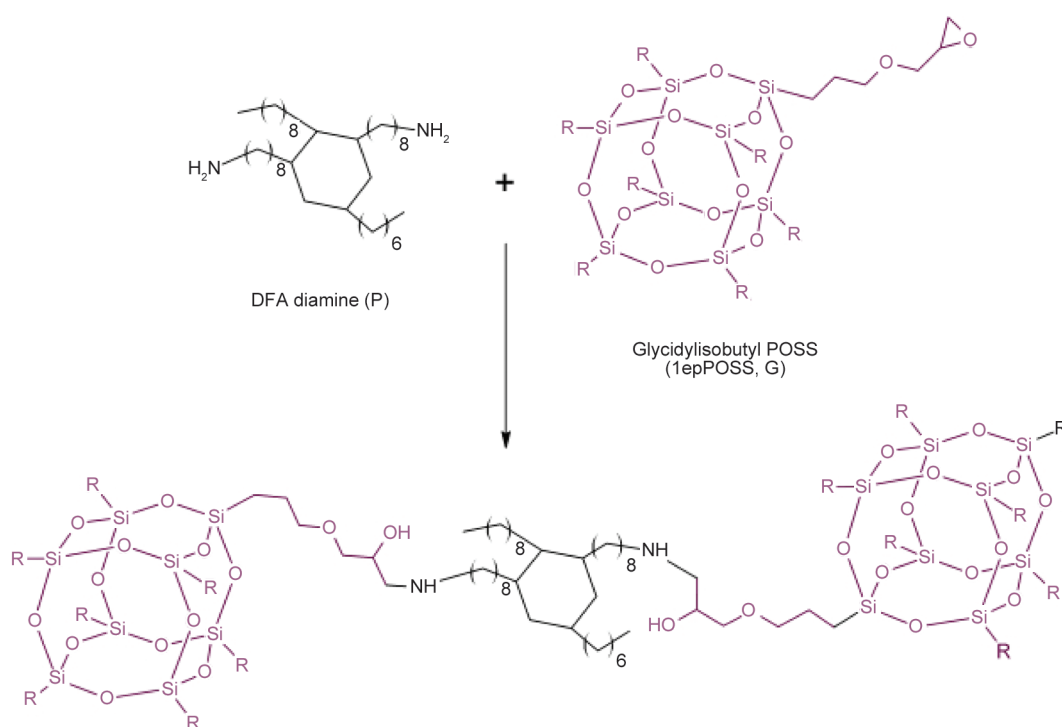


Figure 6. Reaction between DFA diamine (P) and 1epPOSS (G) (epoxy group:amine group = 1 mol:1 mol).

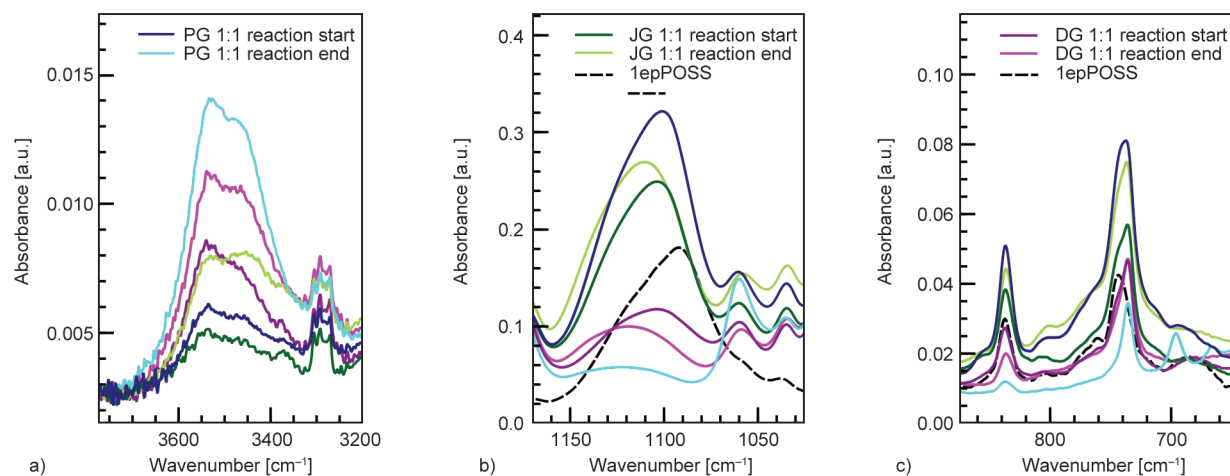


Figure 7. FTIR spectra at various stages of the synthesis of ‘building block’ materials and pure 1epPOSS: a) in the carbonyl region, b) and c) in the epoxy regions. The curves have been translated for clarity.

the reaction between DFA diamine and 1epPOSS (Figure 7c). It is also visible in the reaction between DAB and 1epPOSS. A strong change in the bands intensity at 1100 cm^{-1} is observed. It corresponds to the C–H wagging vibration of the oxirane ring. At the same time, an increase in the intensity of bands around the wavenumber of 3500 cm^{-1} is observed. It is related to the vibrations of –OH groups, which are formed due to the reaction between the oxirane ring and amine groups (Figure 7b). As later shown in NMR studies (Section 3.2. and 3.3.), it is believed that the evident changes to the FTIR spectra visible for the reactions between 1epPOSS particles with epoxy rings and amines (Figure 7) suggest that such a reaction may occur. It is still difficult to state whether it indeed occurs in the environment of the composite synthesis reaction due to several overlapping factors. Overall, it is particularly difficult to detect subtle changes in the FTIR spectra that would indicate oxirane rings reacting with amines while preparing composite materials. There are several inconveniences in reading the spectra – first, the molar mass of 1epPOSS cage compared to the oxirane ring is high, resulting in low intensity of bands from epoxides. Secondly, 1epPOSS concentration in the matrix, in terms of molar ratio (even at 15 wt%), is low, and the reactants are dissolved in the solvent with low concentration (~25 wt%). Finally, overlapping bands from different compounds were observed.

3.2. Hydrogen nuclear magnetic resonance

^1H NMR

Since the FTIR analysis could not give a definite answer whether 1epPOSS was chemically incorporated

into the NIPU structure, it was decided to perform ^1H NMR and ^{13}C NMR experiments.

For a more straightforward determination of the prepolymer spectra, the spectra of raw materials were obtained first. Solutions of amines and carbonate were prepared in deuterated dimethyl sulfoxide (DMSO- d_6) as a solvent Figure 8 [A–C]. However, 1epPOSS was insoluble in DMSO; thus, deuterated pyridine- d_5 was used – Figure 8 [D]. CH_3 groups in isobutyl appear as triplet or *dd* system, which is described in the literature [32]. PPO diamine (J) spectrum shows multiple CH and – CH_2 – groups in close vicinity to oxygen (numerous overlapped multiplets in the region between 3.0–3.6 ppm) [33]. DFA diamine (P) spectrum shows multiple overlapping CH_2 groups in the 1.0–1.3 ppm region. Some – CH_2 – groups (P_c and P_d peaks in Figure 8) are more shifted. Therefore, two left shoulders of this peak were observed [34]. Finally, the TMP tricarboxylate (C) spectrum was obtained. Three highly coupled peaks corresponding to the hydrogen atoms in the vicinity of the carbonate group were observed [35].

The reactions between epoxy groups in 1epPOSS and amines were studied by ^1H NMR in a similar manner as by FTIR. To facilitate solubility, we used the double molar excess of amine groups to obtain amine-terminated low molar mass products. The spectra are presented in Figure 9. A peak at 4–4.5 ppm from the emerging hydroxyl group ($\text{G}_{\text{OH}}^{2^\circ}$ in Figure 9) was observed in all cases. Its existence proves the reaction between all amines and 1epPOSS. As shown in Figure 6, 1epPOSS and amines react by opening the epoxy ring and obtaining a second-order hydroxyl group. Thus $\text{G}_{\text{OH}}^{2^\circ}$ symbol stands for the newly

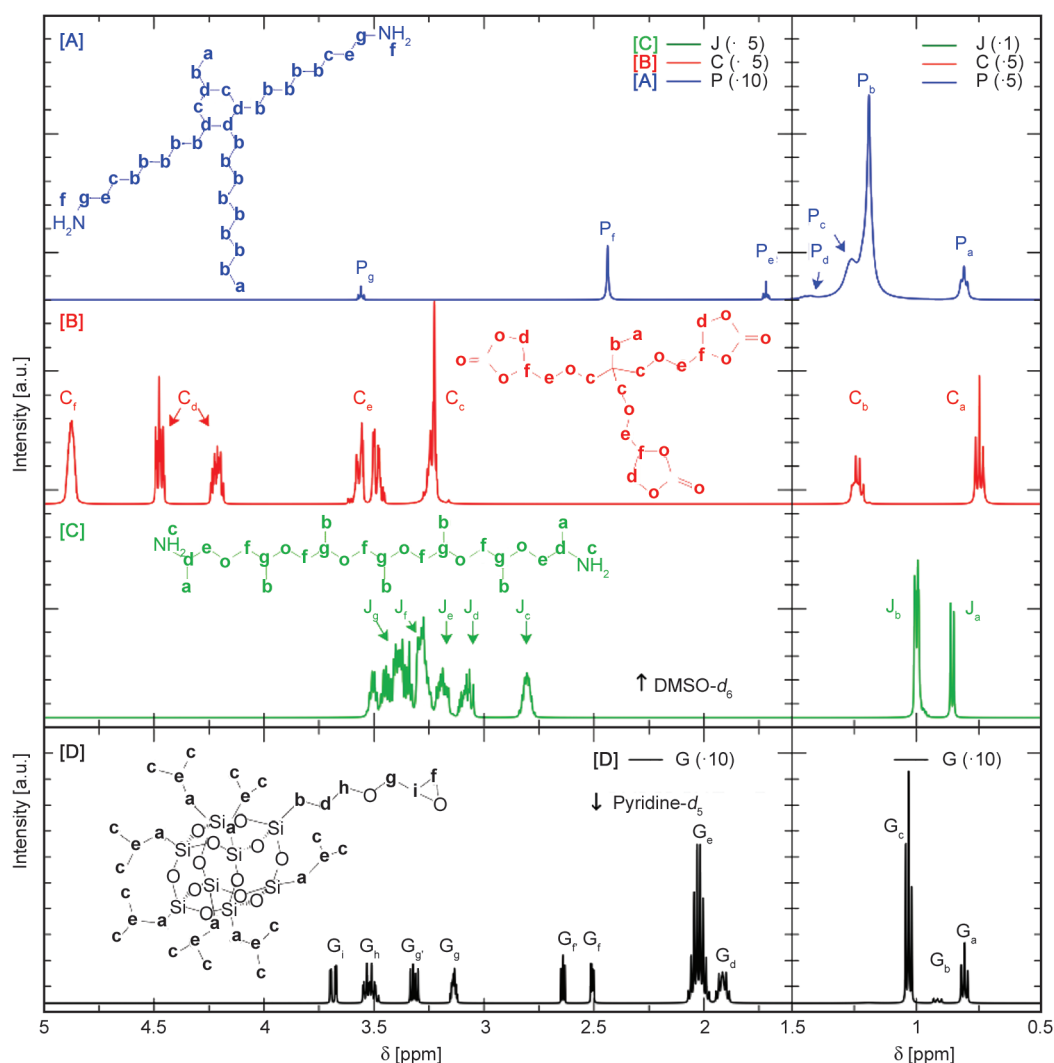


Figure 8. ^1H NMR spectra of raw materials: [A] blue – DFA diamine (P), [B] red – TMP tricarfonate (C), [C] green – PPO diamine (J), [D] black – 1epPOSS (G). Capital letters correspond to the molecule in general, while the lowercase letter in the index corresponds to each hydrogen-containing group in the molecule, as depicted in every molecule's structure by changing the group symbol into a suitable letter. The spectra on the left and right were multiplied for better visibility, which is marked in the graph legend for each spectra. Peaks of the solvents, HDO, and impurities were hidden for the clarity of the image.

emerged second-order hydroxyl groups to distinguish them from the first-order $-\text{OH}$ groups formed during cyclic carbonate aminolysis [36] (Figure 1). Depending on the air-derived moisture concentration in the sample, the peak from hydroxyl groups may be a doublet (Figure 8 [A, B]) or, when the presence of water reduces the coupling, a smooth singlet (Figure 8 [C]). Simultaneously, in low moisture samples, the coupling of the $-\text{NH}_2$ groups is visible (Figure 9 [A]). The excess of amine is visible in peaks denoted P_f , J_c , and D_{NH_2} , which correspond to unreacted amine groups. Unreacted G_i peak, originating from 1epPOSS (marked in black), is visible in the product of the reaction between 1epPOSS and PPO diamine (JG Figure 9 [B]), which indicates a partial reaction

between those two reagents. However, it is not high in intensity, and moreover, the $-\text{CH}_2-$ group in the unreacted epoxy ring denoted as G_f peak, is not visible. In other cases, as mentioned earlier, the lack of the black marked G_i and G_f peaks proves a complete reaction in double molar excess of amine.

Spectra of prepolymers with the highest concentration (15 wt%) of 1epPOSS in $\text{DMSO-}d_6$ are presented in Figure 10. The prominent visible peak is denoted as G_c and originates from multiple CH_3 groups. Due to the low hydrogen amount in 1epPOSS reactive substituents compared to isobutyl substituents and the overall relatively low 1epPOSS concentration in the solution, the peaks originating from smaller hydrogen spin populations are barely

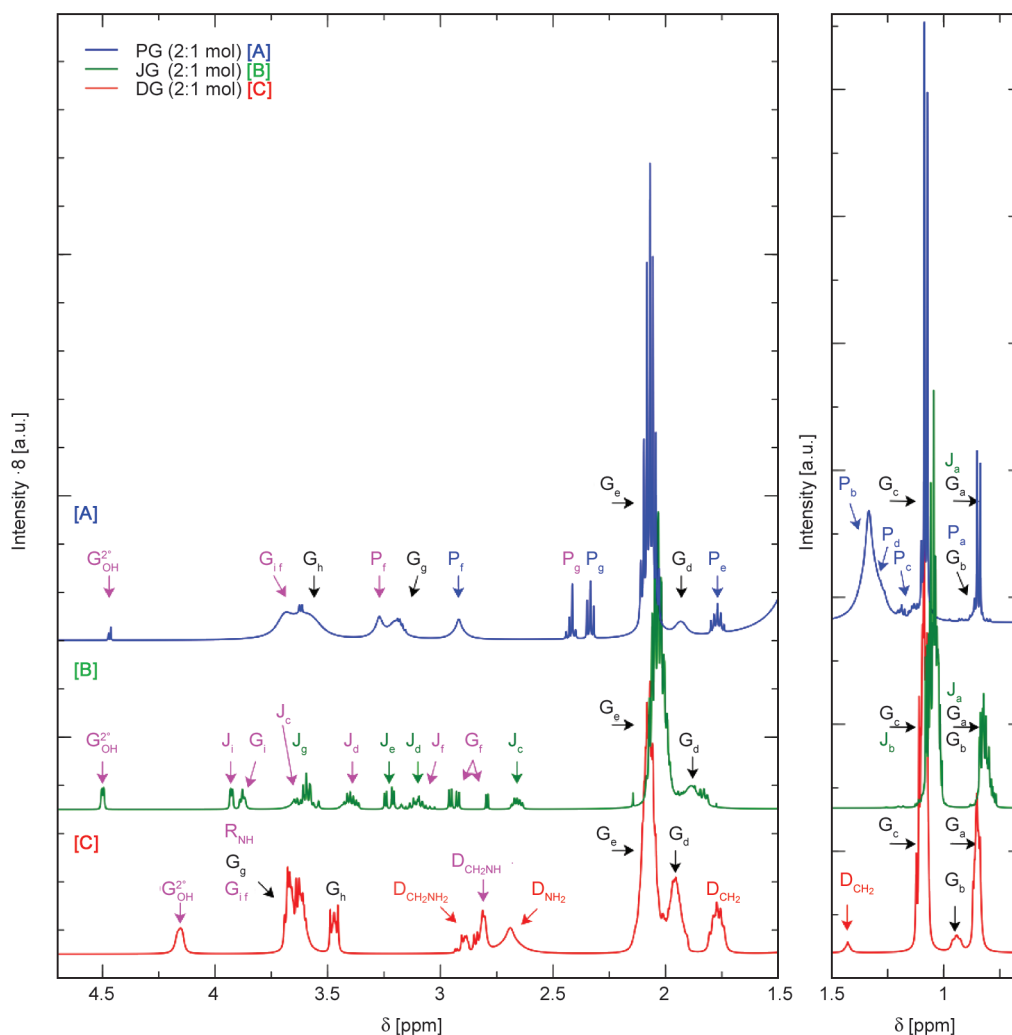


Figure 9. ^1H NMR spectra of 1epPOSS-amine building blocks obtained with a ratio of 2:1 mol of reacting groups: [A] blue PG – DFA diamine (P) with 1epPOSS (G), [B] green JG – PPO diamine (J) with 1epPOSS, [C] red DG – 1,4-diaminobutane (D) with 1epPOSS (G). The notation is the same as in Figure 8. The spectra on the left were multiplied for better visibility. The noise and impurities were removed by fitting Gaussian/Lorentzian model functions to the spectra. Magenta was used for hydrogen atoms directly affected by the reaction and exhibiting entirely new spin populations. $G_{\text{OH}}^{2^\circ}$ stands for the hydroxyl group that emerged during the reaction (see Figure 6).

visible. Thus, peaks originating from epoxy groups and reaction-resulting $-\text{OH}$ groups are masked by overlapping C_{def} and J_{efg} peaks. However, a peak indicating unreacted DFA diamine (a blue P_f singlet that stands out in DFA diamine-containing prepolymers in Figure 10) at around 3 ppm exhibits lower intensity in the case of composites loaded with 15 wt% of 1epPOSS. It can be suggested that 1epPOSS reacts with unreacted amine groups originating from DFA diamine at the end of polymer chains. Interestingly, for PPO diamine, no peaks indicating the presence of unreacted amine groups were observed. J_c peak observed in raw material PPO diamine (Figure 8 [C]) completely converts to J_c magenta in composite materials (Figure 10). Thus, it may be concluded that PPO diamine reacts more readily

with TMP Tricarbonate and 1epPOSS in comparison to DFA diamine. The materials with DFA diamine also differ from PPO diamine-derived materials in signal from urethanes (magenta P_f in Figure 10) at 7 ppm. In DFA diamine-based materials, it has a slightly higher shift and consists of two overlapped signals correlated to urethane-derived $-\text{NH}-$ groups, either reacted or non-reacted with oxirane rings in 1epPOSS. The two signals may result from the spin population formed during the reaction between epoxy groups in 1epPOSS and $-\text{NH}-$ groups in urethanes. Urethanes in which $-\text{NH}-$ groups reacted with epoxy groups in 1epPOSS exhibit lower shift. The peak with a higher shift corresponds to urethanes in which $-\text{NH}-$ groups did not undergo the reaction with epoxy groups in 1epPOSS. The close

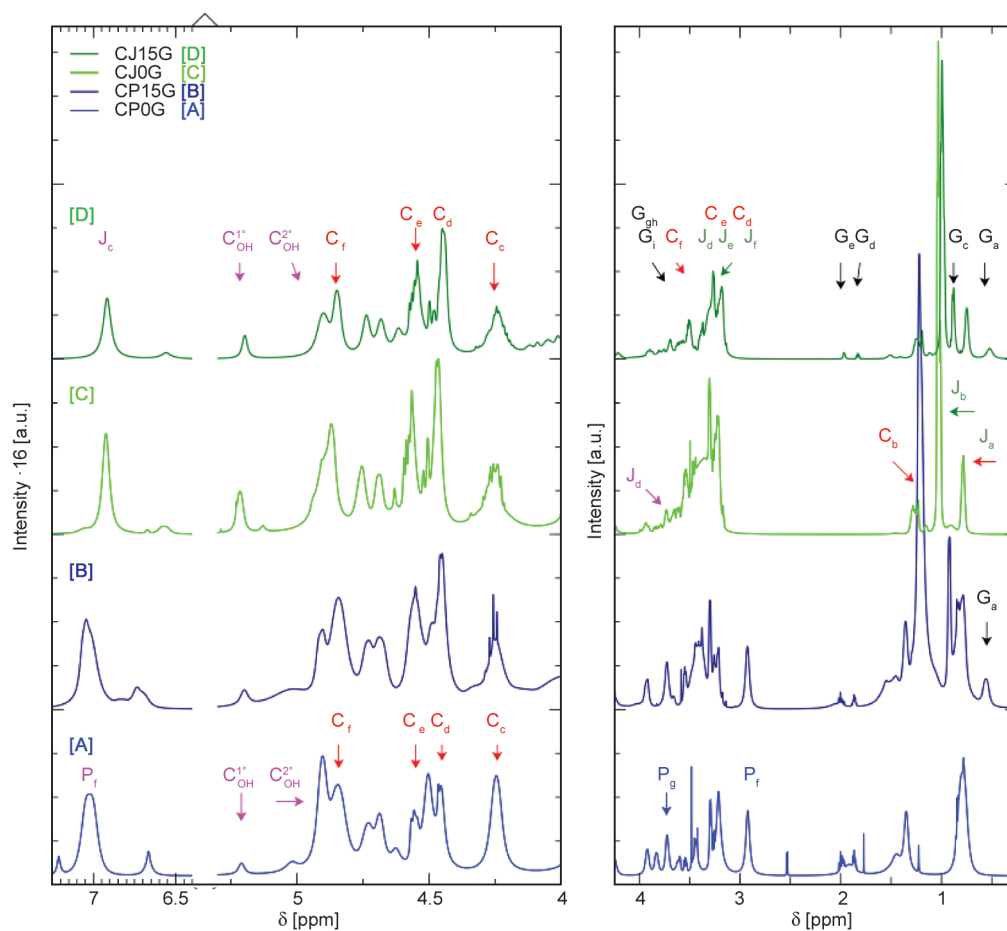


Figure 10. ^1H NMR spectra of obtained prepolymers in $\text{DMSO-}d_6$. The presence of 1epPOSS is denoted by several peaks marked by the letter G in black color. Peaks from water, solvent and impurities were hidden. The notation is the same as in Figure 8.

presence of oxygen, originating from the epoxy group in 1epPOSS, reduces the shift in a similar manner as it is observed in PPO diamine-derived materials. Therefore, the peak from urethanes in which $-\text{NH}-$ group underwent epoxy ring opening reaction may be overlapped entirely with reaction-free urethanes.

3.3. Carbon nuclear magnetic resonance

^{13}C NMR

Spectra of raw materials (after deconvolution and noise reduction) are shown in Figure 11. Peaks were labeled in a similar manner as in the ^1H NMR section: with the symbol of the raw material and ascending letters, which correspond to the carbon atoms in the raw material molecule, as it was shown in Figure 8. Although overlapping of some signals may occur, peak C_g (corresponding to carbonyl group) is visible at 154.5 ppm [37, 38]. Thus, the reaction extent between carbonate and amines can be determined by observing the location of this peak. The shift to

156.5 ppm represents the difference between reacted and unreacted carbonate. The appearance of two peaks in this region would prove the partial reaction of carbonate. Similarly, peaks C_f and C_d (Figure 11, Figure 12) should move to higher shifts due to the reaction progress [15, 39].

The spectra of obtained prepolymers are shown in Figure 12. The observed peaks were labeled in the same manner as in the Figure 8 and Figure 11. The presence of 1epPOSS in materials is clearly denoted by the peaks G_a , G_e , and G_c , which correspond to isobutyl substituents (see Figure 8) [31]. Signals from the reactive epoxy ring are barely visible. However, it is primarily due to being overlapped by other signals. For example, the G_b peak is overlapped by the C_a peak originating from TMP Tricarboxylate (Figure 12). Although low in intensity, the peaks G_f and G_i (magenta Figure 12) were not overlapped and are visible in PPO diamine-based NIPUs at 46 and 66 ppm and DFA diamine-based NIPUs at 58 and 70 ppm, respectively. Those peaks originated

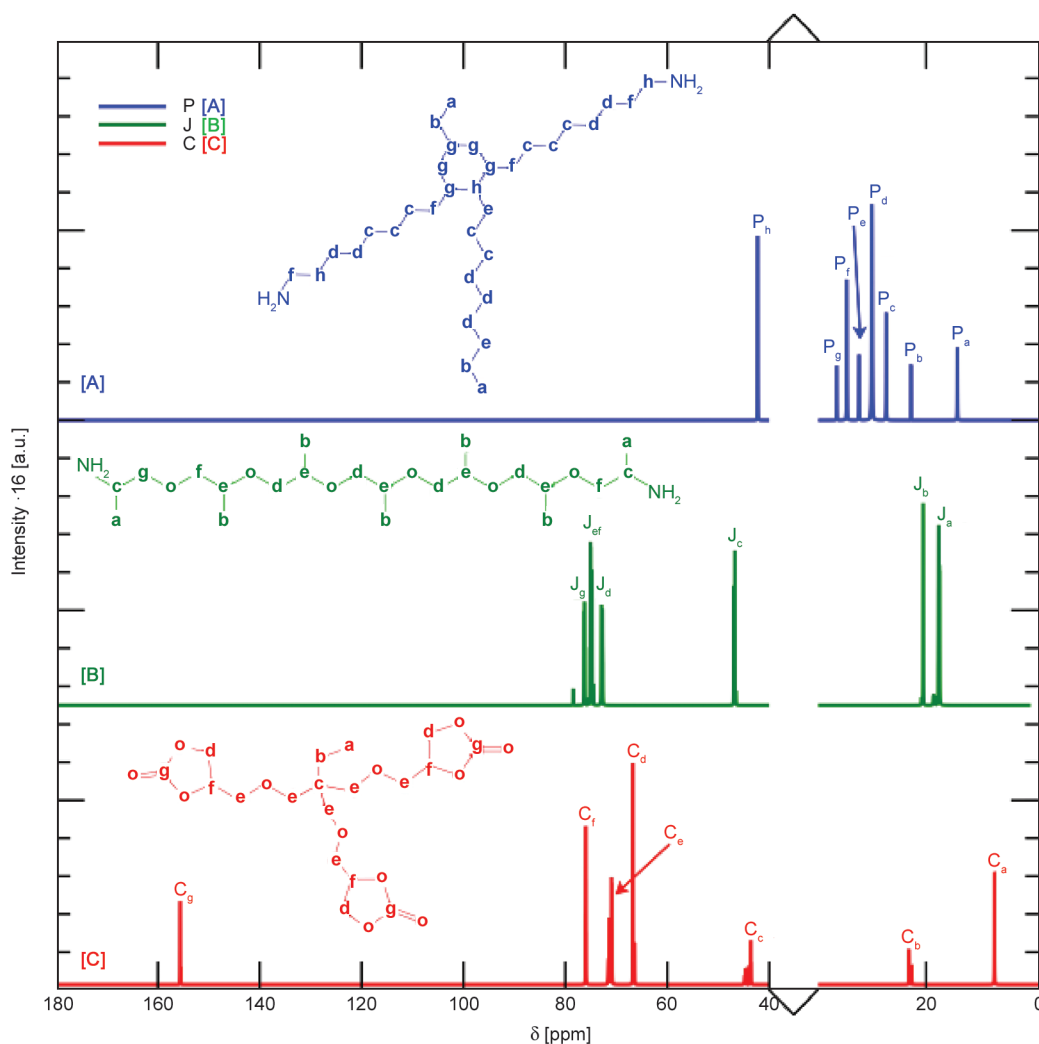


Figure 11. ^{13}C NMR spectra of raw materials used in the synthesis. Capital letters correspond to the molecule in general, while the lowercase letter in the index corresponds to each carbon atom in the molecule as depicted in the structure of every molecule by changing the carbon symbol into a suitable letter.

from the reaction of epoxides with primary amines and, thus, the formation of secondary amines. Thus, they are distinguished with an additional 2°N mark. The presence of those peaks alongside the absence of the peaks G_f and G_i originating from unreacted 1epPOSS (black, 44 and 51 ppm [39]) clearly indicates that the reaction between 1epPOSS and amine also occurs during the prepolymerization.

All prepolymers (Figure 12) exhibit two peaks in the range of urethanes and carbonates (magenta and red peaks C_g), which is expected. Moreover, in all cases, urethane's downfield-shifted peak exhibits higher intensity than the peak from unreacted carbonates. Peak originating from unreacted DFA diamine (blue P_h in Figure 12) is present in all DFA diamine-based materials and has the highest intensity in the respective NIPU matrix. 1epPOSS reacts

with DFA diamine readily, which is supported by the lower intensity of the P_h peak in 1epPOSS-containing samples.

The presence of residual unreacted PPO diamine, denoted by green J_c peak (Figure 12), is also observed in PPO diamine-based materials. However, the corresponding peak has low intensity and does not change in all PPO diamine-based materials. It can be concluded that 1epPOSS introduction does not influence the PPO-amine conversion rate. The peak originating from the reacted amine is also visible as the magenta $J_c^{1,2^\circ\text{OH}}$ peak (Figure 12). It exhibits higher intensity and denotes secondary amines in close vicinity of primary and secondary $-\text{OH}$ groups. The latest may confirm the occurrence of the reaction between amines and both carbonate and epoxy groups.

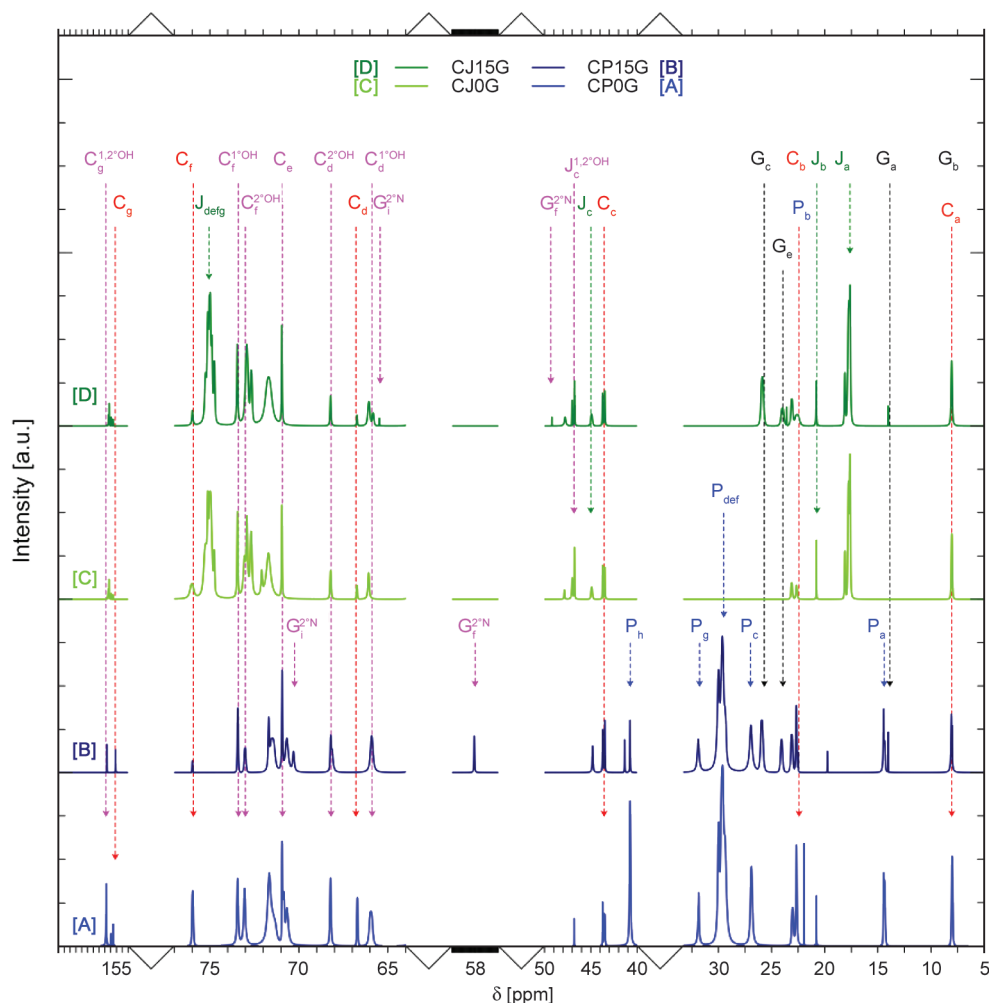


Figure 12. ^{13}C NMR spectra of obtained prepolymers. Peaks from solvent and impurities (DMAc, THF, CH_2Cl_2) were hidden. All prepolymer-derived peaks are labeled in a previous manner: capital letter and color correspond to raw material, while magenta corresponds to either new signals or the ones strongly affected by the reaction; a lowercase letter comes from the particular carbons depicted in Figure 11.

3.4. X-ray diffraction (XRD)

Figure 13 shows diffractograms of the matrices and composites. Only a broad asymmetric amorphous halo is observed for the PPO diamine-based matrix in the 2θ region from 10.0 to 30.0° . Thus, the CJ matrix is believed to be fully amorphous. Similarly, the DFA diamine-based matrix (CP) is also fully amorphous, however, a second, weaker halo is observed at 2θ below 10° , indicating possible inhomogeneity in the nanoscale [40].

For PPO diamine-based composites (Figure 13a), two distinctive Bragg peaks around 7.7 – 8.0° 2θ and 8.6 – 8.9° 2θ are visible. Those peaks originate from 1epPOSS itself (Figure 13c) and likely indicate the presence of 1epPOSS aggregates [25, 41, 42]. For the composite loaded with 5 wt% 1epPOSS, an additional peak is present around 9.5° 2θ . It is not present in the diffractogram of a ‘building block’, *i.e.* a

product of the reaction between PPO diamine and 1epPOSS (JG) (Figure 13c). It may indicate that the PPO diamine-based composite with 5 wt% 1epPOSS loading has a different partial crystalline structure of 1epPOSS contained in the NIPU matrix compared to CJ composites with 10 and 15 wt% 1epPOSS. Another pair of peaks around 2θ 10.7 – 10.9° and 11.6 – 11.9° is visible for PPO diamine-based composites with 10 and 15 wt% 1epPOSS. However, it is not present for composite with 5 wt% 1epPOSS. Those peaks, although slightly shifted, are also present in the diffractogram of its corresponding ‘building block’ (Figure 13c) and most likely come from the presence of 1epPOSS [25, 42, 43]. For PPO diamine-based composites with 10 and 15 wt% 1epPOSS, several crystalline peaks are present over the amorphous halo (10.0 to 30.0° 2θ). Those indicate a more abundant presence of 1epPOSS, which tends

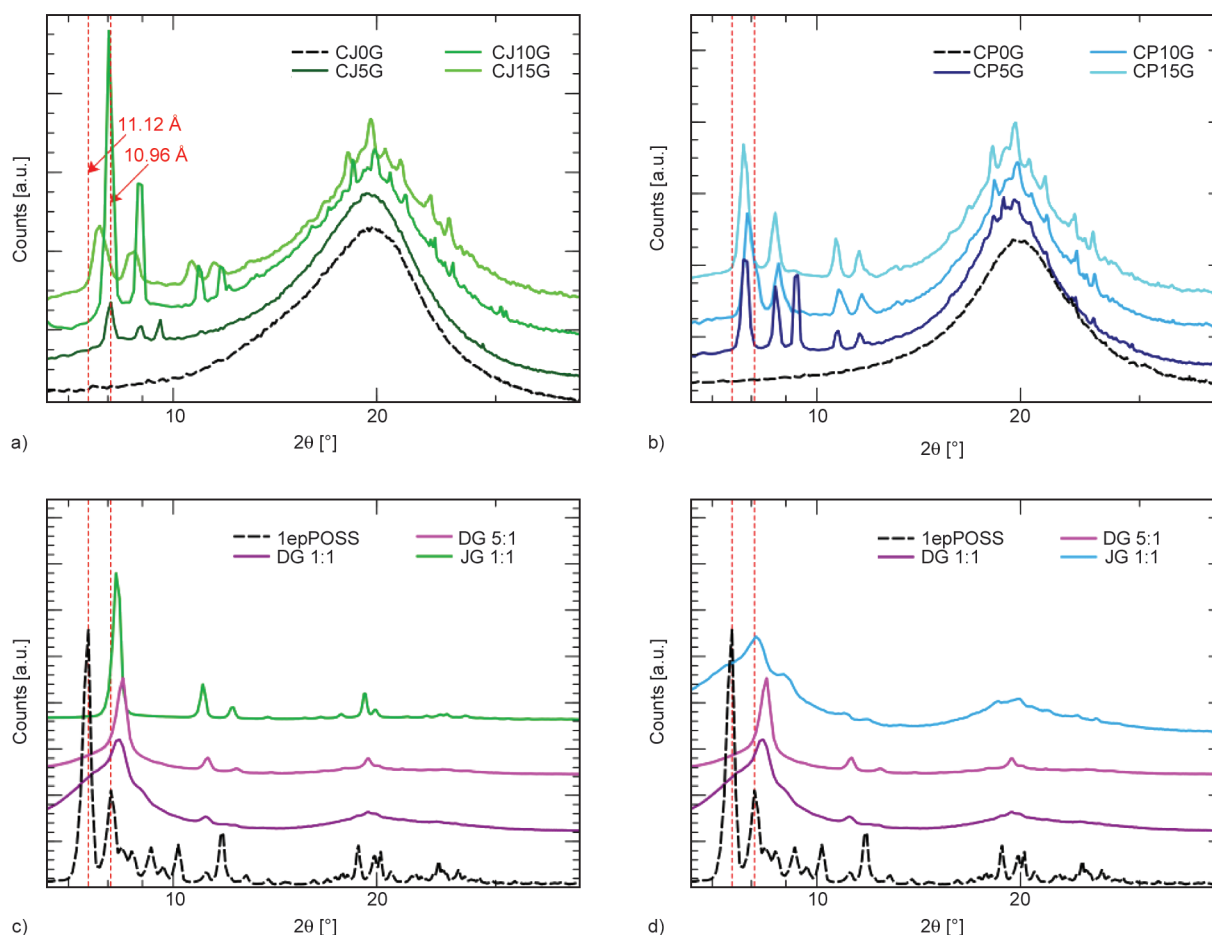


Figure 13. XRD diffractograms of obtained matrices and composites: a) CJ-based materials, b) CP-based materials, as well as ‘building blocks’ materials: c) DG and JG along with 1epPOSS and d) DG and PG along with 1epPOSS.

to agglomerate at those concentrations. It is in accordance with SEM observations (Figure 15) reported in Section 3.5.

Figure 13b shows the diffractograms of DFA diamine-based (P) composites. As for CJ composites, diffractograms of CP composites show a number of corresponding crystalline peaks: a pair around 2θ 7.7–8.0° and 8.6–8.9°, an additional one around 9.5° for 5 wt% 1epPOSS composite, another pair around 10.7–10.9° and 11.6–11.9°, and several crystalline peaks present over the amorphous halo (in the 2θ region of 10–30°). There is a noticeable difference between composites with 5 wt% 1epPOSS based on DFA diamine and PPO diamine. The pair of reflexes around in the 2θ region of 10.7–10.9° and 11.6–11.9° and some crystalline peaks over the amorphous halo region (10.0 to 30.0° 2θ) are visible for DFA diamine-based composite with 5 wt% 1epPOSS. It may indicate that some of the 1epPOSS particles migrated to the surface of the sample.

The presence of crystalline peaks around 9.5° in both composites loaded with 5 wt% 1epPOSS may indicate

that even though 1epPOSS particles were introduced into the reaction at the very beginning, they could react with NIPU matrix in two different ways. Probably due to its low concentration, strong 1epPOSS agglomeration was not facilitated, and thus, the reaction between epoxy rings in 1epPOSS and primary amine groups, as well as newly formed urethane groups, was possible at the same time. It stays in accordance with FTIR analysis in Section 3.1., and NMR study in Sections 3.2 and 3.3.

Figure 13c and Figure 13d show diffractograms of ‘building blocks’ – products of the reaction between 1epPOSS and respective amines used in the synthesis. 1epPOSS is a pure crystalline substance [25, 42, 43], showing several Bragg peaks. Those at 7.5 and 8.0° correspond to distances in 1epPOSS cage, 11.12 Å and 10.96 Å, respectively (Figure 13c and Figure 13d, black) [25, 42, 43]. Those are also visible in composites (although slightly shifted towards higher 2θ values). When 1epPOSS is reacted with DAB in a stoichiometric ratio of reactive groups (Figure 13c and Figure 13d, dark magenta), the

resulting product (DG_1:1) is rather amorphous in nature, showing a distinctive amorphous halo in the range up to around 10.0° 2θ and a couple of peaks at 8.3 , 11.2 and 19.5° 2θ . When 1epPOSS is reacted with DAB with an excess amount of DAB (DG_5:1) (Figure 13c and Figure 13d, light magenta), the resulting product becomes less amorphous, as the visible amorphous halo decreases in width and crystalline peaks become more intense. The products of the reaction between 1epPOSS and PPO diamine (J) or DFA diamine (P) differ in their crystalline nature. JG_1:1 (Figure 13c, green) is a highly crystalline substance with no distinctive amorphous halo visible and crystalline reflexes in the 2θ range of 8.0 – 20.0° . It is also probably due to the nature of PPO diamine, which is a diamine based on poly(propylene oxide) – a semi-crystalline substance itself [43, 44, 45]. PG_1:1 (Figure 13d, blue) bears similarity to DG_1:1 – it is rather amorphous in nature, showing two distinctive amorphous halos in the range up to around 10.0° and from 14.5 to 30.0° as well as a few Bragg peaks in the 2θ range of 8.0 – 20.0° . PG_1:1 is based on DFA diamine, which is a deriviate of dimmer fatty acid – an aliphatic, amorphous substance [46, 47].

3.5. SEM microscopy

SEM images were taken for composite materials, loaded with increasing 1epPOSS content (5–15 wt%) (Figure 14, Figure 15). As one can notice in Figure 13,

1epPOSS is a crystalline substance [25, 39, 40]. Presumably, crystalline 1epPOSS agglomerates of few micrometers in size may be observed. At the same time, some 1epPOSS seem to be well dispersed with the NIPU matrices, which is indicated by Si being detected in the whole area of the SEM image [48].

Figure 14 shows SEM images of composites based on DFA diamine with different 1epPOSS content. With increasing 1epPOSS content from 5 to 10 wt%, the amount of visible 1epPOSS agglomerates also increases, while their size and shape (roughly circular/spherical) stays unchanged. At the same time, silicon is visible in the whole area of the image, indicating uniform dispersion for a substantial fraction of the additive. When the composite is loaded with 15 wt% of 1epPOSS, it tends to form larger agglomerates, which become irregular in shape.

Figure 15 shows SEM images of composites based on PPO diamine (J), with different 1epPOSS content. CJ-based composites are similar to those based on the CP matrix, with the exception that some 1epPOSS clusters emerge already at 5 wt% of 1epPOSS content and are more substantial in size. Still, up to 10 wt% of 1epPOSS, Si is present in the whole imaged area, indicating good dispersion for the major part of 1epPOSS particles. As for the DFA diamine-based composite, a large amount of irregularly-shaped clusters is visible at 15 wt% 1epPOSS content for the composite based on PPO diamine. Here,

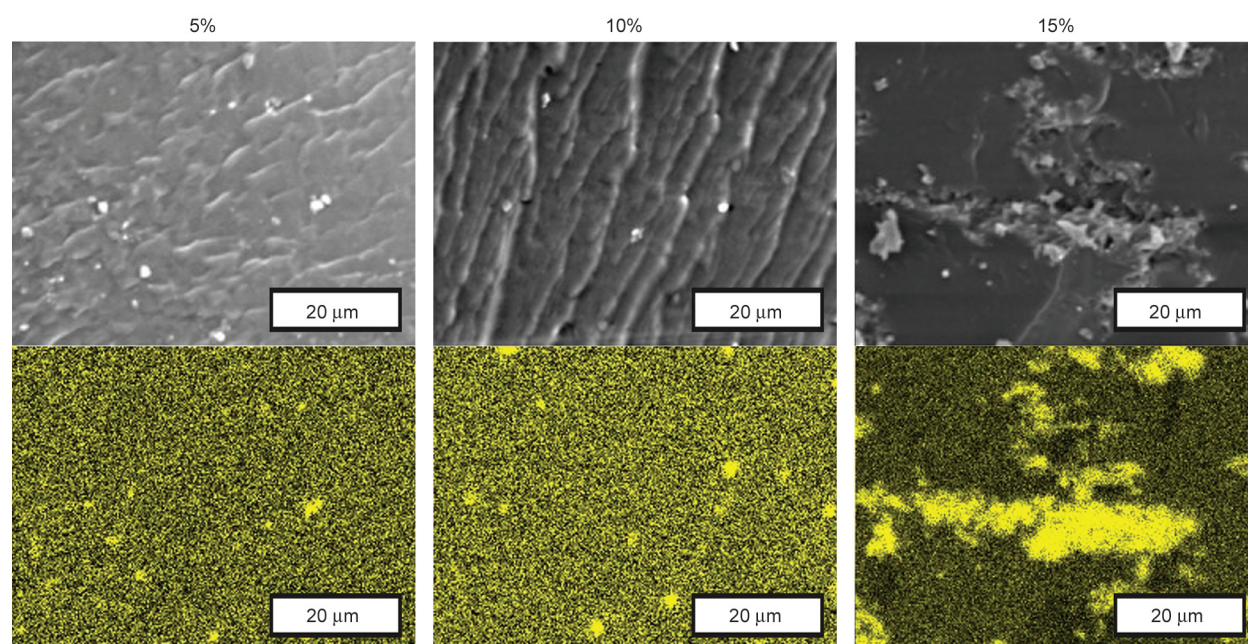


Figure 14. SEM images of surfaces produced by cryofracturing NIPU composites based on DFA diamine, with different 1epPOSS content (5–15 wt%) along with corresponding silicon EDS (yellow heat maps). Scale bars correspond to 20 μm .

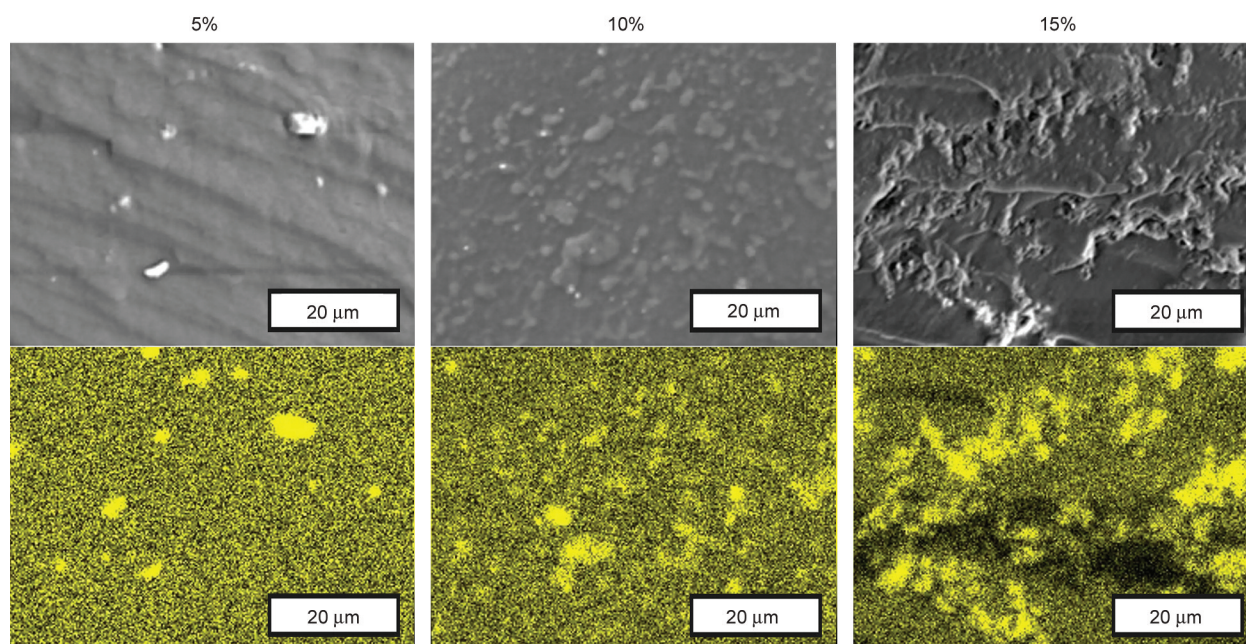


Figure 15. SEM images of surfaces produced by cryofracturing NIPU composites based on PPO diamine, with different 1epPOSS content (5–15 wt%) along with corresponding silicon EDS (yellow heat maps). Scale bars correspond to 20 μm .

some areas where silicon is not detected are present, meaning that the dispersion of the remaining 1epPOSS particles is deteriorated. Based on EDS maps, 1epPOSS distribution in DFA diamine-based composites seems to be better in comparison to PPO diamine-based ones. Not only is silicon present in the whole observed area, but also the emerging 1epPOSS agglomerates are smaller and regular in shape, even for the highest 1epPOSS content.

3.6. Dynamic mechanical analysis

Dynamic Mechanical Analysis was conducted to assess the mechanical properties of obtained samples and observe the influence of 1epPOSS addition on the behavior of NIPU network. The DMA curves are shown in Figure 16. The main features of the DMA curves are: a step in storage modulus (E'); accompanied by a peak in $\tan\delta$. This effect is related to the α relaxation, *i.e.* the dynamic glass transition. The peak in $\tan\delta$, is a good measure of the glass transition temperature (T_g) of the material. This temperature (T_α) and the glassy modulus (E'_g), *i.e.* the value of E' at a temperature below T_α are plotted for both series in Figure 17 as a function of 1epPOSS content.

The first interesting observation is related to the characteristics of the pure networks themselves. DFA diamine-based matrix exhibits lower T_α than PPO diamine-based matrix (Figure 17), which corresponds

to increased mobility. It is also interesting to note that α relaxation for the DFA diamine-based matrix is accompanied by a smaller contribution on its high-temperature side, as observed in the $\tan\delta$ curves (Figure 16c). The presence of a second peak may indicate a degree of inhomogeneity in the DFA diamine-based matrix, which was also observed on the basis of XRD analysis (Section 3.4.). The difference in T_α between the two matrices may indicate that polymer chains in the CP-based network are not as tightly packed as in the CJ-based one. The above originates from the different natures of amine backbones. Long hydrocarbon side chains present in DFA diamine likely cause steric hindrance, effectively creating free space in the polymer network. On the contrary, the linear PPO chains are easier to pack, reducing free space. For the same reason, the CJ-based matrix also has almost 3 times higher glassy modulus than its CP-based counterpart (Figure 17b). Also, the formation of hydrogen bonds may occur more readily within CJ-based materials due to the abundance of oxygen in PPO diamine-derived segments. The glassy plateau region for CP-matrix is visible in the temperature range of 60 to -10°C (Figure 16a), whereas for CJ-matrix, it reaches further up to 10°C (Figure 16b), all due to differences in amine composition of the polymer network. For both of the matrices, a drop of storage modulus and a breakage of the sample around 60°C is observed.

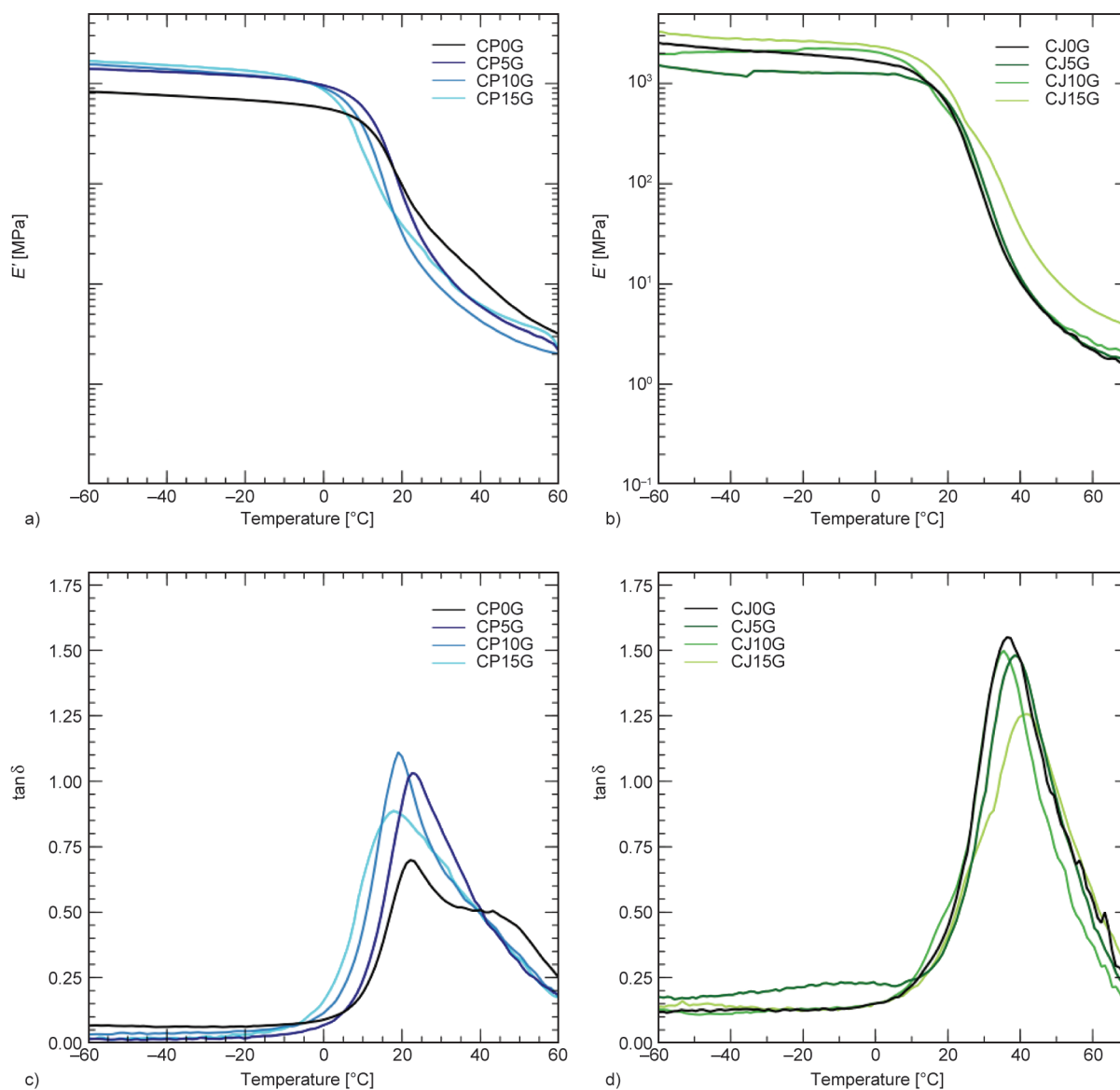


Figure 16. DMA measurement results obtained for NIPU matrices and composites with different 1epPOSS content (5–15 wt%): a) E' for DFA diamine-based materials (CP); b) E' for PPO diamine-based materials (CJ); c) $\tan \delta$ for DFA diamine-based materials (CP); d) $\tan \delta$ for PPO diamine-based materials (CJ) as a function of temperature.

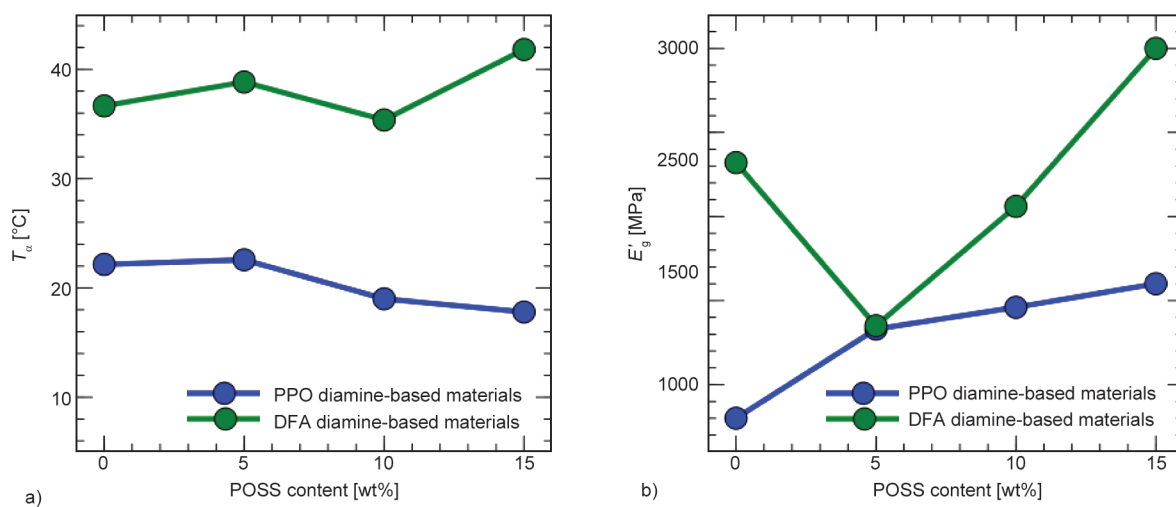


Figure 17. The dependence of: a) T_g and b) E'_g on 1epPOSS content for obtained NIPU materials.

Figure 16a shows DMA curves obtained for DFA diamine-based materials (CP). The plots of $\tan \delta$ vs. temperature show distinctive peaks, indicating their respective T_{α} , as shown in Figure 17a. With increasing 1epPOSS content in composites, the T_{α} values decrease. A shift of $\tan \delta$ peaks of composites towards lower temperatures with increasing 1epPOSS content, the increase in their intensity and the narrowing of their shape is visible for all 1epPOSS loads. Those changes are the indication of the loosening of the NIPU networks and facilitated polymer chain mobility. 1epPOSS particles bear only one reactive vertex group (epoxy), as seen in Figure 6. When reacting with amines, 1epPOSS terminate chain growth of NIPU matrix, interrupting cross-linking and leading to the loosening of the polymer network. Some unreacted 1epPOSS particles may also facilitate the effect of loosening of NIPU network. The formation of 1epPOSS agglomerates, observed in SEM-EDS images (Figure 14, Figure 15), especially for higher 1epPOSS loads (15 wt%), may be an additional cause of the aforementioned phenomenon [49]. At -50°C , the composites exhibit glassy moduli, as shown in Figure 17b. The glassy modulus of CP-based materials increases with increasing 1epPOSS content. Significant enhancement is observed, as DFA diamine-based matrix (CP) is less mechanically resistant than the PPO diamine-based (CJ) one. The observed reinforcement in the values of E' occurs probably due to siliceous 1epPOSS particles in the NIPU matrix, and most probably due to the formation of 1epPOSS nanocrystals already observed in XRD diffractograms (Figure 13) and SEM-EDS images (Figure 14, Figure 15).

DMA curves obtained for PPO diamine-based composites are presented in Figure 16b. The trend of T_{α} changes is not linear. Only the addition of 5 or 15 wt% of 1epPOSS causes the increase of T_{α} . This is an interesting observation. In reference [49], the very same materials were studied with differential scanning calorimetry (DSC) and dielectric relaxation spectroscopy (DRS). Calorimetric T_g showed a decrease with increasing 1epPOSS content. However, the Arrhenius traces, as determined by DRS, showed an inversion of the trends around 0.1 Hz, *i.e.* above this frequency, the temperature of the Arrhenius trace was at higher temperatures with increasing 1epPOSS content. This was attributed to radical changes in cooperativity. Here, the experiment was done at 1 Hz, *i.e.* above the crossover. As for the reinforcement of

the glassy modulus in PPO diamine-based composites, it is only visible in the case of composite loaded with 15 wt% of 1epPOSS. When the PPO diamine-based matrix (CJ) is modified with enough 1epPOSS particles – here 15 wt% – only then the reinforcing effect of the presence of siliceous 1epPOSS particles overpowers the effect of loosening the polymer network, overall strengthening the matrix. The glassy modulus shows a peculiar behavior with increasing 1epPOSS content (Figure 17b). An initial drop at 5 wt% is followed by a continuous increase. This might be related to two opposing effects. The first one is the loosening of the polymer network, which seems to be dominant for smaller 1epPOSS contents. Above 5 wt%, this is counteracted by the reinforcing effect of the siliceous 1epPOSS particles.

3.7. Static stretching test

Static stretching test was performed to further study the mechanical properties of the obtained materials and to analyze the influence of 1epPOSS addition on their performance. Figure 18 shows stress-strain curves obtained for matrices and NIPU-1epPOSS composites. Table 2 shows corresponding numerical data – tensile strength and elongation at break.

DFA diamine-based matrix exhibited tensile strength over 3 times greater than the matrix based on PPO diamine at room temperature (Table 2). As mentioned in Section 3.6, the differences in tensile strength between the two NIPU matrices originate from the composition of amine backbones. Contrary to the dynamic nature of the thermo-mechanical test in DMA, during the static stretching test, long hydrocarbon main- and side chains present in DFA diamine present higher tensile resistance to applied force. The linear poly(propylene oxide) chains in PPO diamine are easier to pack, thus reducing the free volume, they are less flexible and, in turn, less mechanically resistant [44–48, 50, 51]. The above-mentioned trend is also visible in the obtained elongation at break values (Table 2).

The influence of 1epPOSS addition on the mechanical properties of DFA diamine-based composites seems not to be beneficial. A notable decrease in tensile strength is exhibited by the sample filled with 10 wt% of 1epPOSS. Other CP-based NIPU-1epPOSS composites have their tensile strength lowered by a lesser degree. Although the numerical values can not be compared directly, this trend is in accordance with the DMA study. The storage modulus

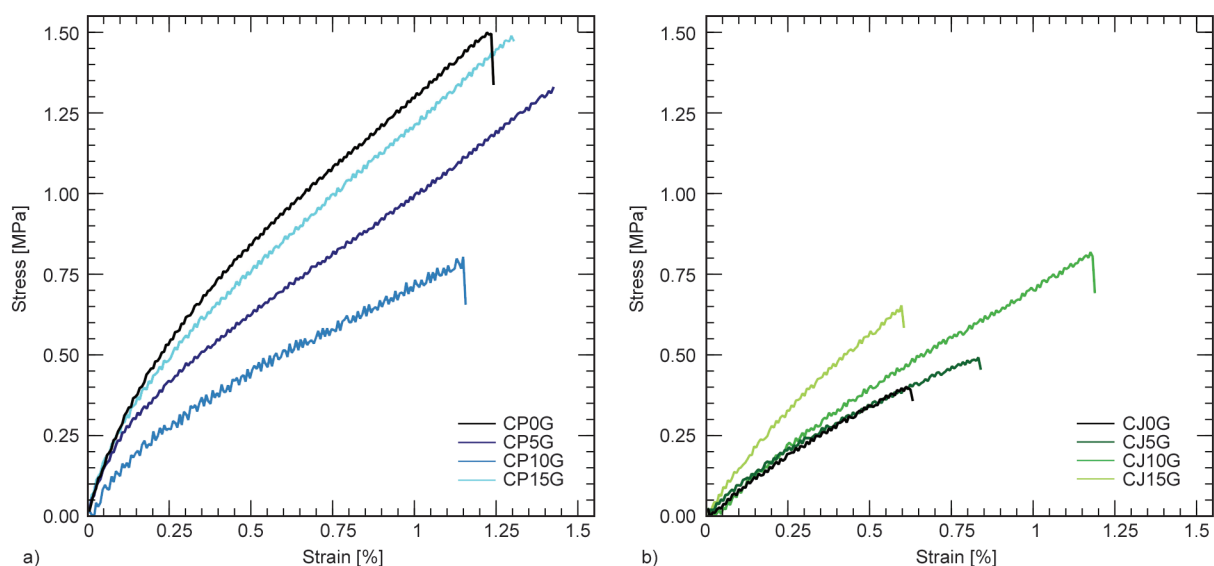


Figure 18. Static stretching test results for NIPU matrices and composites with different 1epPOSS content (5–15 wt%) based on: a) DFA diamine and b) PPO diamine.

Table 2. Mechanical parameters of obtained NIPU-1epPOSS hybrid materials.

Sample name	Tensile strength [MPa]	Elongation at break [%]	$E'_{25^{\circ}\text{C}}$ [MPa]
CP0G	1,50	124	45
CP5G	1,32	142	26
CP10G	0,80	116	15
CP15G	1,49	130	23
CJ0G	0,40	63	218
CJ5G	0,49	84	284
CJ10G	0,82	118	234
CJ15G	0,65	60	43

recorded at 25 °C ($E'_{25^{\circ}\text{C}}$) decreases slightly for samples filled with 5 and 15 wt% of 1epPOSS, and a significant decrease is visible for the CP10G sample in comparison to pristine CP0G matrix (Table 2). The presence of monofunctional 1epPOSS in CP-based NIPU-1epPOSS composites disrupts cross-linking, leading to the loosening of the polymer network and, in turn, to a decrease in mechanical strength.

On the contrary to CP-based composites, the addition of 1epPOSS to PPO diamine-based NIPU-1epPOSS composites facilitates the increase in both tensile strength and elongation at break in all obtained samples (Table 2). The most prominent reinforcement (two fold) is noted for the sample filled with 10 wt% of 1epPOSS. Less mechanically resistant CJ-based NIPU matrix benefits from the reinforcing effect of the presence of siliceous 1epPOSS particles. Despite loosening the polymer network, the presence of more mechanically resistant 1epPOSS cages in the

structures of CJ-1epPOSS composites influences the overall tensile resistance of the studied materials to a greater extent. In turn, at room temperature, the summary effect of those two contradicting phenomena results in an increase in both tensile strength and elongation at break [22–25]. In the case of CJ-based composites, the trend between storage modulus recorded at 25 °C obtained from the DMA study and tensile strength obtained from the static stretching test is not preserved (Table 2). Nevertheless, it is worth noting that the CJ 1epPOSS composite sample filled with 15 wt% of 1epPOSS shows increased mechanical properties in comparison to the unmodified CJ matrix in both sub-ambient (glassy) (E'_g at -50°C) and room (elastic) temperature ($E'_{25^{\circ}\text{C}}$ and tensile strength) conditions (Table 2).

4. Conclusions

Non-isocyanate polyurethanes (NIPUs) were successfully obtained via polyaddition of diamines with five membered tri(cyclic carbonate) in a two-step process. NIPU-1epPOSS nanocomposites were synthesized without the use of toxic isocyanates, staying in accordance with green chemistry rules. FTIR analysis confirmed that almost all carbonate groups were converted into urethane groups after the chain extension step of the synthesis, ensuring a high conversion rate. Observation of direct changes in the FTIR spectra that would indicate the opening of epoxy rings present in 1epPOSS via the reaction with amines (or any other groups known from their reactivity towards epoxy rings) during the synthesis of composite

materials proved to be difficult. Yet, FTIR analysis confirmed 1epPOSS reactivity towards used amines. Results obtained using another spectroscopic method – ^1H NMR – stay in accordance with FTIR data – the occurrence of the reaction between amines and carbonate, resulting in the formation of HNIPU, was confirmed. It can be suggested that the used 1epPOSS is reacting with unreacted amine groups originating from DFA diamine at the end of polymer chains. Importantly, based on ^{13}C NMR analysis, it was clearly indicated that the reaction between 1epPOSS and amine also occurs in the prepolymerization step during the synthesis of composite materials.

NIPU-1epPOSS composites where low 1epPOSS concentration (5 wt%) was applied facilitated better 1epPOSS distribution as revealed by WAXD results. SEM-EDS analysis indicated that although 1epPOSS agglomeration occurred more readily with increasing 1epPOSS content, overall uniform dispersion for a substantial part of 1epPOSS particles was observed, especially for low 1epPOSS concentrations (5 wt%). Additionally, a better distribution of 1epPOSS in the NIPU matrix was achieved for DFA diamine-based composites.

Dynamic mechanical analysis data revealed the differences between DFA diamine-based and PPO diamine-based matrices' thermo-mechanical behavior, most probably originating from the different structures of the chains of respective amines used in the synthesis. An extended study is needed to fully assess the effect of 1epPOSS influence on T_α for PPO diamine-based composites, however, an effect of loosening of the NIPU network by the addition of 1epPOSS was observed for DFA diamine-based composites. In general, the presence of 1epPOSS proved to be beneficial in terms of mechanical reinforcement for DFA diamine-based composite materials. The reinforcement effect was also noted for PPO diamine-based NIPU materials at 15 wt% of 1epPOSS loading.

Further mechanical studies revealed that the addition of 1epPOSS particles influences the studied NIPU composite materials in a different way, depending on the amine used in the preparation of individual matrices. Inherently more mechanically resistant CP-based NIPU matrix exhibits lowered tensile strength in its composites upon the addition of 1epPOSS particles. On the other hand, when added to less mechanically tough PPO diamine-based NIPU materials,

1epPOSS particles have a beneficial effect in terms of tensile strength as well as elongation at break values, which is confirmed by both DMA and static stretching tests.

These results confirm that it is possible to fabricate tailor-made isocyanate-free polyurethane reinforced by 1epPOSS as organic-inorganic sustainable hybrid materials with a tunable thermo-mechanical response.

Acknowledgements

This work was supported by the Polish National Science Center under Contract No. 2017/27/B/ST8/01584.

References

- [1] Bizet B., Grau É., Cramail H., Asua J. M.: Water-based non-isocyanate polyurethane-ureas (NIPUUs). *Polymer Chemistry*, **11**, 3786–3799 (2020).
<https://doi.org/10.1039/D0PY00427H>
- [2] Pistor V., de Conto D., Ornaghi F. G., Zattera A. J.: Microstructure and crystallization kinetics of polyurethane thermoplastics containing trisilanol isobutyl POSS. *Journal of Nanomaterials*, **2012**, 283031 (2012).
<https://doi.org/10.1155/2012/283031>
- [3] Mapp C. E., Corona P. C., De Marzo N., Fabbri L.: Persistent asthma due to isocyanates: A follow-up study of subjects with occupational asthma due to toluene diisocyanate (TDI). *American Review of Respiratory Disease*, **137**, 1326–1329 (1988).
<https://doi.org/10.1164/ajrccm/137.6.1326>
- [4] Wisnewski A. V., Xu L., Robinson E., Liu J., Redlich C. A., Herrick C. A.: Immune sensitization to methylene diphenyl diisocyanate (MDI) resulting from skin exposure: Albumin as a carrier protein connecting skin exposure to subsequent respiratory responses. *Journal of Occupational Medicine and Toxicology*, **6**, 6 (2011).
<https://doi.org/10.1186/1745-6673-6-6>
- [5] Lemi re C., Romeo P., Chaboillez S., Tremblay C., Malo J.-L.: Airway inflammation and functional changes after exposure to different concentrations of isocyanates. *Journal of Allergy and Clinical Immunology*, **110**, 641–646 (2002).
<https://doi.org/10.1067/mai.2002.128806>
- [6] Vijayan V. K.: Methyl isocyanate (MIC) exposure and its consequences on human health at Bhopal. *International Journal of Environmental Studies*, **67**, 637–653 (2010).
<https://doi.org/10.1080/00207233.2010.515435>
- [7] Bello D., Woskie S. R., Streicher R. P., Liu Y., Stowe M. H., Eisen E. A., Ellenbecker M. J., Sparer J., Youngs F., Cullen M. R., Redlich C. A.: Polyisocyanates in occupational environments: A critical review of exposure limits and metrics. *American Journal of Industrial Medicine*, **46**, 480–491 (2004).
<https://doi.org/10.1002/ajim.20076>

- [8] Liu Y., Stowe M. H., Bello D., Woskie S. R., Sparer J., Gore R., Youngs F., Cullen M. R., Redlich C. A.: Respiratory protection from isocyanate exposure in the autobody repair and refinishing industry. *Journal of Occupational and Environmental Hygiene*, **3**, 234–249 (2006).
<https://doi.org/10.1080/15459620600628704>
- [9] Boros R. Z., Koós T., Wafaa C., Nehéz K., Farkas L., Viskolcz B., Szőri M.: A theoretical study on the phosgenation of methylene diphenyl diamine (MDA). *Chemical Physics Letters*, **706**, 568–576 (2018).
<https://doi.org/10.1016/j.cplett.2018.06.024>
- [10] Chen L., Wu D., Kim J-M., Yoon J.: An ESIPT-based fluorescence probe for colorimetric, ratiometric, and selective detection of phosgene in solutions and the gas phase. *Analytical Chemistry*, **89**, 12596–12601 (2017).
<https://doi.org/10.1021/acs.analchem.7b03988>
- [11] Rokicki G., Parzuchowski P. G., Mazurek M.: Non-isocyanate polyurethanes: Synthesis, properties, and applications. *Polymers for Advanced Technologies*, **26**, 707–761 (2015).
<https://doi.org/10.1002/pat.3522>
- [12] Chaturvedi D.: Perspectives on the synthesis of organic carbamates. *Tetrahedron*, **68**, 15–45 (2012).
<https://doi.org/10.1016/j.tet.2011.10.001>
- [13] Sedlák M., Pejchal V., Imramovský A., Hanusek J.: A safe and efficient route for the preparation of nitro-, dinitro-, and trinitrophenyl chloroformates. *Synthetic Communications*, **43**, 2365–2369 (2013).
<https://doi.org/10.1080/00397911.2012.709300>
- [14] Suryawanshi Y., Sanap P., Wani V.: Advances in the synthesis of non-isocyanate polyurethanes. *Polymer Bulletin*, **76**, 3233–3246 (2019).
<https://doi.org/10.1007/s00289-018-2531-7>
- [15] Chen Z., Hadjichristidis N., Feng X., Gnanou Y.: Poly(urethane-carbonate)s from carbon dioxide. *Macromolecules*, **50**, 2320–2328 (2017).
<https://doi.org/10.1021/acs.macromol.7b00142>
- [16] Schmitz F., Keul H., Höcker H.: Alternating copolymers of tetramethylene urea with 2,2-dimethyltrimethylene carbonate and ethylene carbonate; Preparation of the corresponding polyurethanes. *Macromolecular Rapid Communications*, **18**, 699–706 (1997).
<https://doi.org/10.1002/marc.1997.030180811>
- [17] Błażek K., Datta J.: Renewable natural resources as green alternative substrates to obtain bio-based non-isocyanate polyurethanes-review. *Critical Reviews in Environmental Science and Technology*, **49**, 173–211 (2019).
<https://doi.org/10.1080/10643389.2018.1537741>
- [18] Guan J., Song Y., Lin Y., Yin X., Zuo M., Zhao Y., Tao X., Zheng Q.: Progress in study of non-isocyanate polyurethane. *Industrial and Engineering Chemistry Research*, **50**, 6517–6527 (2011).
<https://doi.org/10.1021/ie101995j>
- [19] Birukov O., Potashnikova R., Leykin A., Figovsky O., Shapovalov L.: Advantages in chemistry and technology of non-isocyanate polyurethane. *Scientific Israel-Technological Advantages*, **16**, 92–102 (2014).
- [20] Špírková M., Kubin M., Dušek K.: Side reactions in the formation of polyurethanes: Stability of reaction products of phenyl isocyanate. *Journal of Macromolecular Science*, **27**, 509–522 (1990).
<https://doi.org/10.1080/00222339009349572>
- [21] Maisonneuve L., Lamarzelle O., Rix E., Grau E., Cramail H.: Isocyanate-free routes to polyurethanes and poly(hydroxy urethane)s. *Chemical Reviews*, **115**, 12407–12439 (2015).
<https://doi.org/10.1021/acs.chemrev.5b00355>
- [22] Blattmann H., Mülhaupt R.: Multifunctional POSS cyclic carbonates and non-isocyanate polyhydroxyurethane hybrid materials. *Macromolecules*, **49**, 742–751 (2016).
<https://doi.org/10.1021/acs.macromol.5b02560>
- [23] Liu G., Wu G., Chen J., Kong Z.: Synthesis, modification and properties of rosin-based non-isocyanate polyurethanes coatings. *Progress in Organic Coatings*, **101**, 461–467 (2016).
<https://doi.org/10.1016/j.porgcoat.2016.09.019>
- [24] Liu G., Wu G., Chen J., Huo S., Jin C., Kong Z.: Synthesis and properties of POSS-containing gallic acid-based non-isocyanate polyurethanes coatings. *Polymer Degradation and Stability*, **121**, 247–252 (2015).
<https://doi.org/10.1016/j.polymdegradstab.2015.09.013>
- [25] Pielichowski K., Njuguna J., Janowski B., Pielichowski J.: Polyhedral oligomeric silsesquioxanes (POSS)-containing nanohybrid polymers. *Advances in Polymer Science*, **201**, 225–296 (2006).
https://doi.org/10.1007/12_077
- [26] Ghanbari H., Cousins B. G., Seifalian A. M.: A nanocage for nanomedicine: Polyhedral oligomeric silsesquioxane (POSS). *Macromolecular Rapid Communications*, **32**, 1032–1046 (2011).
<https://doi.org/10.1002/marc.201100126>
- [27] Ozimek J., Pielichowski K.: Recent advances in polyurethane/POSS hybrids for biomedical applications. *Molecules*, **27**, 40 (2022).
<https://doi.org/10.3390/molecules27010040>
- [28] CRODA: Technical data sheet Priamine™ 1074 (2016).
- [29] Huntsman: Technical data sheet JEFFAMINE® D-400 Polyetheramine (2019).
- [30] Blain M., Jean-Gérard L., Auvergne R., Benazet D., Caillol S., Andrioletti B.: Rational investigations in the ring opening of cyclic carbonates by amines. *Green Chemistry*, **16**, 4286–4291 (2014).
<https://doi.org/10.1039/C4GC01032A>
- [31] Wang T., Deng H., Li N., Xie F., Shi H., Wu M., Zhang C.: Mechanically strong non-isocyanate polyurethane thermosets from cyclic carbonate linseed oil. *Green Chemistry*, **24**, 8355–8366 (2022).
<https://doi.org/10.1039/D2GC02910C>

- [32] Ye M., Wu Y., Zhang W., Yang R.: Synthesis of incompletely caged silsesquioxane (T7-POSS) compounds via a versatile three-step approach. *Research on Chemical Intermediates*, **44**, 4277–4294 (2018).
<https://doi.org/10.1007/s11164-018-3368-2>
- [33] Siddiqi H. M., Dumon M., Pascault J. P.: Polymer-dispersed liquid crystals: Liquid crystal/polymer composites as electro-active materials. in ‘Proceedings of 3rd International Conference on Intelligent Materials and 3rd European Conference on Smart Structures and Materials. Lyon, France’ Vol. 2779, 435–440 (1996).
<https://doi.org/10.1117/12.237157>
- [34] Kebir N., Nouigues S., Moranne P., Burel F.: Nonisocyanate thermoplastic polyurethane elastomers based on poly(ethylene glycol) prepared through the transesterification approach. *Journal of Applied Polymer Science*, **134**, 44991 (2017).
<https://doi.org/10.1002/app.44991>
- [35] Cornille A., Dworakowska S., Bogdal D., Boutevin B., Caillol S.: A new way of creating cellular polyurethane materials: NIPU foams. *European Polymer Journal*, **66**, 129–138 (2015).
<https://doi.org/10.1016/j.eurpolymj.2015.01.034>
- [36] Błażek K., Kasprzyk P., Datta J.: Diamine derivatives of dimerized fatty acids and bio-based polyether polyol as sustainable platforms for the synthesis of non-isocyanate polyurethanes. *Polymer*, **205**, 122768 (2020).
<https://doi.org/10.1016/j.polymer.2020.122768>
- [37] Specific polymers: Technical data sheet TMP tricyclo-carbonate (2010).
- [38] Pathak R., Kathalewar M., Wazarkar K., Sabnis A.: Non-isocyanate polyurethane (NIPU) from tris-2-hydroxy ethyl isocyanurate modified fatty acid for coating applications. *Progress in Organic Coatings*, **89**, 160–169 (2015).
<https://doi.org/10.1016/j.porgcoat.2015.08.015>
- [39] Błażek K., Beneš H., Walterová Z., Abbrent S., Eceiza A., Calvo-Correas T., Datta J.: Synthesis and structural characterization of bio-based bis(cyclic carbonate)s for the preparation of non-isocyanate polyurethanes. *Polymer Chemistry*, **12**, 1643–1652 (2021).
<https://doi.org/10.1039/D0PY01576H>
- [40] Shen Z., Zheng L., Li C., Liu G., Xiao Y., Wu S., Liu J., Zhang B.: A comparison of non-isocyanate and HDI-based poly(ether urethane): Structure and properties. *Polymer*, **175**, 186–194 (2019).
<https://doi.org/10.1016/j.polymer.2019.05.010>
- [41] Perrin F. X., Nguyen T. B. V., Margailan A.: Linear and branched alkyl substituted octakis(dimethylsiloxy)octasilsesquioxanes: WAXS and thermal properties. *European Polymer Journal*, **47**, 1370–1382 (2011).
<https://doi.org/10.1016/j.eurpolymj.2011.04.004>
- [42] Franchini E., Galy J., Gérard J-F., Tabuani D., Medici A.: Influence of POSS structure on the fire retardant properties of epoxy hybrid networks. *Polymer Degradation and Stability*, **94**, 1728–1736 (2009).
<https://doi.org/10.1016/j.polymdegradstab.2009.06.025>
- [43] Nagendra B., Cozzolino A., Daniel C., Rizzo P., Guerra G., Auriemma F., De Rosa C., D’Alterio M. D., Tarallo O., Nuzzo A.: Two nanoporous crystalline forms of poly(2,6-dimethyl-1,4-phenylene)oxide and related co-crystalline forms. *Macromolecules*, **52**, 9646–9656 (2019).
<https://doi.org/10.1021/acs.macromol.9b01911>
- [44] Golla M., Cozzolino A., Nagendra B., Vignola E., Daniel C., Rizzo P., Guerra G., Auriemma F., D’Alterio M. C.: Molecular features behind formation of α or β I-crystalline and nanoporous-crystalline phases of PPO. *Frontiers in Chemistry*, **9**, 809850 (2022).
<https://doi.org/10.3389/fchem.2021.809850>
- [45] Li Y., Shimizu H.: Novel morphologies of poly(phenylene oxide) (PPO)/polyamide 6 (PA6) blend nanocomposites. *Polymer*, **45**, 7381–7388 (2004).
<https://doi.org/10.1016/j.polymer.2004.09.018>
- [46] Younes G. R., Maric M.: Increasing the hydrophobicity of hybrid poly(propylene glycol)-based polyhydroxyurethanes by capping with hydrophobic diamine. *Industrial and Engineering Chemistry Research*, **60**, 8159–8171 (2021).
<https://doi.org/10.1021/acs.iecr.1c01293>
- [47] Zhao W., Liang W., Feng Z., Xue B., Xiong C., Duan C., Ni Y.: New kind of lignin/polyhydroxyurethane composite: Green synthesis, smart properties, promising applications, and good reprocessability and recyclability. *ACS Applied Materials and Interfaces*, **13**, 28938–28948 (2021).
<https://doi.org/10.1021/acsami.1c06822>
- [48] Raftopoulos K. N., Łukaszevska I., Calduch C. B., Stachak P., Lalik S., Hebda E., Marzec M., Pielichowski K.: Hydration and glass transition of hybrid non-isocyanate polyurethanes with POSS inclusions. *Polymer*, **253**, 125010 (2022).
<https://doi.org/10.1016/j.polymer.2022.125010>
- [49] Raftopoulos K. N., Pielichowski K.: Segmental dynamics in hybrid polymer/POSS nanomaterials. *Progress in Polymer Science*, **52**, 136–187 (2016).
<https://doi.org/10.1016/j.progpolymsci.2015.01.003>
- [50] Zhou Z., Su X., Liu J., Liu R.: Synthesis of vanillin-based polyimine vitrimers with excellent reprocessability, fast chemical degradability, and adhesion. *ACS Applied Polymer Materials*, **2**, 5716–5725 (2020).
<https://doi.org/10.1021/acsapm.0c01008>
- [51] Yang G., Fu S-Y., Yang J-P.: Preparation and mechanical properties of modified epoxy resins with flexible diamines. *Polymer*, **48**, 302–310 (2007).
<https://doi.org/10.1016/j.polymer.2006.11.031>